Spring 1-1-2018

Experimental Validation for the Theory of Blisters' Instabilities

Hongtian Zhu
University of Colorado at Boulder, hozh1629@colorado.edu

Experimental Validation for the Theory of Blisters' Instabilities

by

Hongtian Zhu

B.S. Harbin Institute of Technology, 2016

A thesis submitted to the

Faculty of the Graduate School of the

University of Colorado in partial fulfillment

of the requirement for the degree of

Master of Science

Department of Mechanical Engineering

2018

This thesis entitled:

Experimental Validation for the Theory of Blisters' Instabilities

written by Hongtian Zhu

has been approved for the Department of Mechanical Engineering

_____

(Franck J. Vernerey)

_____

(Rong Long)

_____

(Francisco López Jiménez)

Date_____

The final copy of this thesis has been examined by the signatories, and we find that both the content and the form meet acceptable presentation standards of scholarly work in the above-mentioned discipline

Zhu, Hongtian (M.S., Department of Mechanical Engineering)

Experimental Validation for the Theory of Blisters' Instabilities

Thesis directed by Associate Professor Franck J. Vernerey

Abstract

Blister formation is a universal problem that can be witnessed within a wide range of contents. It is first documented as a side effect of syringomyelia and other diseases. Later on, the forming of blisters are also observed during the cell apoptosis, which leads to the hypothesis that it could have some intricate relationships with the death of living organisms. Other than biological problems, blister forming is also a common phenomenon in thin film technologies. Therefore, the research in the forming of blisters is essential and critical in both engineering and science fields.

In this thesis, we study the problem of a growing blister made of a rubber-like membrane adhered on a rigid substrate, and the implications that it might have on possible artificial shape-morphing skins. We show that a blister test is a problem driven by competition between two instabilities: one inherent to the rubber, and second one pertaining to the adhesion with the substrate. This enables obtaining different results with such that the final blister profile can be perfectly controlled by only adjusting the thickness of the film and the inflation rate. Given the theory, the rest part of this thesis is mainly focused on the experimental validation of it. We designed our unique experimental systems to analyze such problem and by matching the experimental results and simulation results, we can verify the validity of our theory.

Acknowledgments

This thesis is under the supervision of Associate Professor Franck J. Vernerey. During my 2-years' study, he gave me a lot of valuable advice which carries me through the jungle of research. And every time I encountered a difficulty, he would always be in his office and willing to help. I would like to thank him from the bottom of my heart for his intelligence, kindness, and patience that helped me and guided me through such a wonderful journey. In the meantime, I also want to express my gratitude to my other committee members, Assistant Professor Rong Long and Assistant Professor Francisco López Jiménez, for devoting their precious time in giving me valuable feedbacks towards this thesis.

I would like to give a special thanks to Ph.D. candidate Eduard Benet Cerda for helping me writing the theory part of this thesis and giving me useful suggestions about my experiments. The time I spent with him was delightful and thank you for being such an awesome co-worker. Meanwhile, I would like to thank Tong Shen, who helped me searching the right direction for my thesis. I also want to thank my former and current lab mates, Shankar Lalitha Sridhar, Kanghyeon Koo, Robert Wagner, Zachary White, Jian Kan, Revathi Priyanka Mohan, Emily Volk, Millicent Gabriel, and Kelly Gazarik who were so kind to me. They were always there to offer support when I needed extra help. My time with them was so memorable. I feel so lucky to know them in Vernerey's Group.

Apart from academic life, I have met so many friends via different opportunities, some are from classes, some are from Theta Tau fraternity, some are from International Coffee Hour, some are from soccer pitches, etc. All the people I know are the best ones that I have ever met in my life. Thank you all for making my life brighter and filled with joy!

This thesis is dedicated to my father, mother, and all of my family members who support me all the time. Even though they are in another hemisphere, I can still feel their warmth. They are the backbone of my spirit and my soul gains strength from their nourishment. I could not express more about how grateful I am for them, and I know it will take me forever to reciprocate their love.

Table of Contents

List of Tables

List of Figures

Chapter 1

Introduction

1.1 Motivation

Camouflaging is a strategy evolved through millions of years for some animal species to survive in nature. It is an important technique for various them to conduct as ways of avoiding predators, catching preys, or even mating. Lots of camouflaging is achieved by changing the morphology of their skins, mimicking themselves of rocks, corals, or other species, etc. These animals' skins are specialized with multiple scattered blister-like protrusions via a set of distributed papillae. This allows them to change their skins at will. One good example is the Common Octopus (*Octopus vulgaris*), it has the ability to change the morphology within a second using muscular hydrostatic mechanism [1]. In this case, the forming of blisters is induced into the protrusion of the octopus' epidermis. Even though the phenomenon has drawn wide attention, the mechanics behind it still needs further investigation.

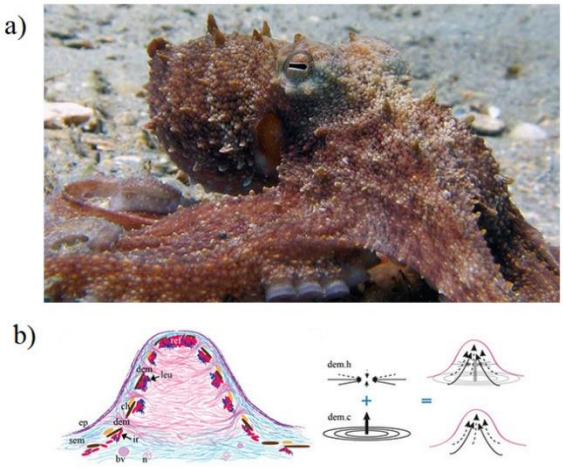

Fig.1-1. a) Octopus mimicking a stone. b) The scheme of papillae

The forming of blisters, or blebs, is quite common in nature. It is well observed during cell apoptosis [2] and budding among the yeasts. Besides biology, the interest of blister has shown far beyond as they are commonly encountered in a variety of situations, in both science and engineering. For example, in medicine, they are seen in the agglutination of erythrocytes by polylysine.[3] In industrial applications, blisters appear in protective thin films such as paint [4] or are used to study the adhesion properties between two materials [5]. Recent research has also taken advantage of this process to study the dissolution of graphene [6] and the properties of soft dielectric membranes [7].

1.2 Current stage

Lots of researches have been done on blister forming. Early as the beginning of the 20th century, researchers started to look into the blisters' formation in syringomyelia [8] and in other diseases [9,10]. In the 1930s, Hahn, et al, first researched on skin blisters [11]. However, those researches either took blisters as a 'side product' of those diseases and did not quite look into them. Then, in 1957 [12], people started to examine the mechanics of blister formation, but mostly in a pathological or biochemical pathway, the mechanics behind remained unclear yet. As time goes by, with the development of human technology, people started to look into the blisters on the lead electrode of lead-acid batteries [13]. Lots of observations and researches are done on a material level, which mostly focuses on the chemistry side, but some started to research the mechanics of blister formation [14]. Starting in the 1980s, due to the growth of new materials and a new test method called blister test [15], which is used to analyze the adhesion between different materials, people eagerly need to build a mathematical model for the development of blisters. Farris et al. [16] analyzed the blister formation as an interface crack problem and Kinloch et al. [17] introduced a method to determine adhesion using surface energy and fracture

mechanics, and a preliminary mathematical model of peeling is given. After that, Williams et al. [5] further examined the scenario and gave mathematical derivations. In the paper, a mechanical model of peeling an adhesive membrane off a rigid substrate is constructed and the derivation is given. Besides them, tones of works have been done in the related area. For example, Gent et al. [18], Chang et al. [19], Kendall et al. [20], researched the adhesion mechanics. Hinkley et al. [15], Wan et al. [21], researched on blister test and fracture mechanics. Those are the people who promoted the research of blister formation to a brand-new level and also built a solid foundation for our work described in this thesis.

1.3 Drawbacks of current research and our novelty

Lots of progress has been made over the last several decades, but one drawback of previous research is that all those findings are based on rigid materials like SiO_2 or graphene. Those materials are almost unstretchable. Meanwhile, the research on the blisters formed by flexible and stretchable materials still remains insufficient. Dating back to the beginning of the blister researches, the reason it firstly draws attention is that it can be found on the human epidermis and as is known to all that human skins are soft and stretchable. Therefore, the research on those premises is critical and necessary. Our research focuses majorly on the mechanics behind the blisters formed by a stretchable membrane and, to accommodate it with the material property, the instability of such blebs.

Other than lack of compensating the component of soft materials in such research, another important factor should also be considered, which is the viscoelasticity. It is very common in biological tissues [22], hence such a feature should not be neglected within the context of this thesis. Viscoelasticity is a quite complex problem and this thesis is the first in this field to

combine the viscoelasticity of material and the blister growing problem together. Even though there are quite a lot of papers that examined the viscoelastic properties dating back to 1935 [23], only a few took the blister into account. Roy et al. [24] researched the thin film delamination while the material is viscoelastic. It is close to what we are examining but the material they tested was a thin film of epoxy instead of rubber-like materials that can undergo huge deformation.

This research on blisters is quite rewardable. One the one hand, such research will shed a light on understanding the mechanics behind the blister forming on the cell membranes, especially in cell apoptosis. By analyzing different parameters, and link them with former biochemical and pathological studies, we can peek into the physiological reasons of how blisters forming and what may cause the mechanical property to change. On the other hand, the mechanism also has a wide application in an engineering context. For example, new technologies based on blisters has shown huge potential in the next generation of LCE displays [25], The formation of blisters can also be utilized in actuation of soft robots [26] or next generation of camouflage system just like what octopuses do. This research will broaden the human knowledge of blisters in general and have huge potentials of being utilized in engineering purposes.

1.4 Objectives

The objective of this thesis is to use experimental methods to validate an analytical model that can predict the behavior of blister growing which is made out of either hyperelastic material or viscoelastic material.

1.5 Thesis scope and organization

This thesis is organized into 4 subsequent chapters. Chapter 1 provides a brief introduction to the thesis, including the background, current research results and the main tasks. In Chapter 2, we will investigate the problem and analyze it, following with the introduction of the mathematical and physical foundation of the problem. Chapter 3 deals with the experimental validation, including the experimental setup and the procedure. We tested EcoFlex^{TM} 00-30 silicon rubber as the sample of hyperelastic material and 3M^{TM} VHB tape as the sample of viscoelastic material. Finally, Chapter 4 exhibits the conclusion by combining the experimental results and theoretical simulation together to show the validation of the theory.

Chapter 2

Theory Foundation

2.1 Initial analyzation

The formation of blisters on biological tissues is intrinsically a complicated problem. Therefore, to simplify the problem and maximize the efficiency of simulation, we hereby study the problem of a growing blister made from rubber-like membrane adhered on a rigid substrate. Fig. 2-1 demonstrates the scenario.

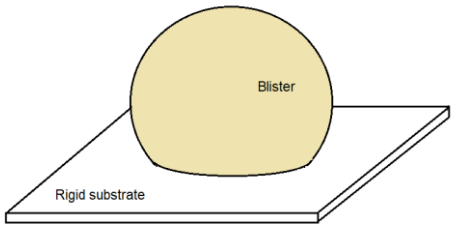

Fig.2-1. Simplification of the problem

2.2 Property of rubber-like membrane

2.2.1 Rubber

Rubber, which was first discovered as a natural material, has been used throughout human history. Dated back to Maya and Aztec cultures, people use the rubber to make balls, containers and waterproof coating for textiles. In 1909, a team headed by Fritz Hofmann, working at the Bayer laboratory in Elberfeld, Germany, succeeded in polymerizing Isoprene, which is known as the first synthetic rubber. During WWI and WWII, synthetic rubber has been widely explored and developed due to intense demand during the war. From then on, a large variety of

rubber has been designed and put into massive production which has influenced our lives till now.

a) Incompressibility

If we hold a piece of rubber and try to deform it, we will find that it is easier to change the shape than to change the volume. In this aspect, the rubber behaves like liquid. Hence, in good approximation, rubber is usually considered as an incompressible material. Fig. 2-2 describes the deformation of solids.

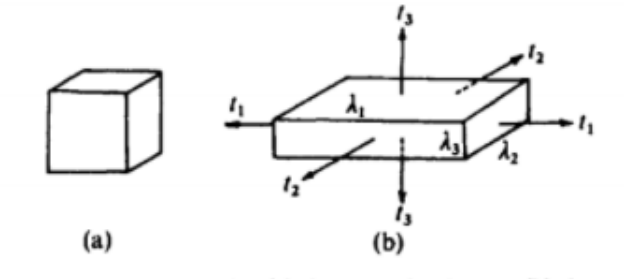

Fig.2-2. Bulk deformation of solids

If we assume the height, length, and width of the original material are x_0, y_0, z_0, then we can obtain the deformed dimensions are:

$$\begin{aligned} x_1 &= \lambda_1 x_0 \\ y_1 &= \lambda_2 y_0 \\ z_1 &= \lambda_3 z_0 \end{aligned} \tag{2.1}$$

Meanwhile, we know the volume is not changed during the deformation, which is $V = V_0$, hence we have the following equation:

$$V = x_1 y_1 z_1 = \lambda_1 \lambda_2 \lambda_3 x_0 y_0 z_0 = x_0 y_0 z_0 = V_0 \tag{2.2}$$

Therefore, we can obtain: $\lambda_1\lambda_2\lambda_3 = 1$. This is the incompressibility equation of any incompressible solid.

b) Microscopic model of rubber

Rubber is a type of polymer, it follows the basic microscopic structure of polymers. They are long string-like molecules made of certain chemical units called 'monomer' [27]. Fig. 2-3 below shows the relationship between monomer, polymer and polymer network, which consists of so-called 'cross-linker' to interconnect same or different polymers.

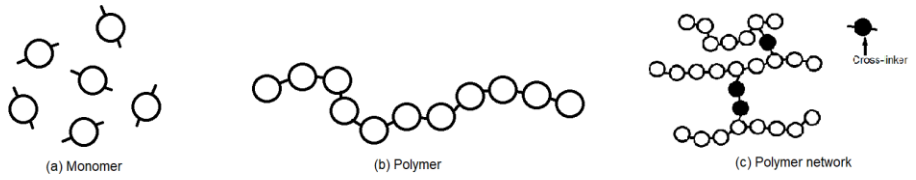

Fig.2-3. Relationship between monomer, polymer and polymer network

To better understand the property of rubber, people use freely joint chain model to describe the microscopic behavior of polymer molecules. As is known to all that the polymer molecules are flexible, it acts as a string in many ways. Fig. 2-4 shows the freely joint chain model. In freely joint chain model, a polymer molecule is represented as N segments with a unique length b, here b is known as Kuhn length. Between each segment, a flexible joint is used to connect each other. Such joint only prevents the translation in all axis (x, y, and z), but let the rotation along them free.

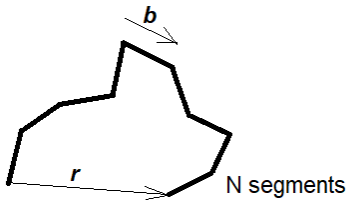

Fig.2-4. Freely joint chain model

To discuss the elasticity of polymer chain using freely joint chain model, we need to consider the end-to-end vector r and the force f exerted on one end of the chain (here we assume the other end is fixed in position). When $\boldsymbol{f} = 0$, the distribution of **r** is isotropic, hence the average of **r**, <**r**> is equal to 0. To simplify the analyzation, we consider the average <$\mathbf{r}^2$> .

Assume $\mathbf{b_n}$ (n=1,2,…,N) is the end-to-end vector of each Kuhn length, therefore the end-to-end vector of the polymer chain **r** is

$$\boldsymbol{r} = \sum_{n=1}^{N} \boldsymbol{b_n} \tag{2.3}$$

From that, we can obtain the square of <***r***> as

$$< \boldsymbol{r^2} >= \sum_{n=1}^{N}\sum_{m=1}^{N} < \boldsymbol{b_n} \cdot \boldsymbol{b_m} > \tag{2.4}$$

For randomly distributed segments, the $\boldsymbol{b_n}$ are independent of each other, hence we have

$$< \boldsymbol{b_n} \cdot \boldsymbol{b_m} >= \delta_{mn}\boldsymbol{b^2} \tag{2.5}$$

So, we have $< \boldsymbol{r^2} >= \sum_{n=1}^{N} < \boldsymbol{b_n}^{\boldsymbol{2}} > = Nb^2$, the average of ***r*** then can be derived as

$$< \boldsymbol{r} >= \sqrt{N}\boldsymbol{b} \tag{2.6}$$

Because the maximum length for a single polymer chain is $r_{max} = Nb$, the maximum elongation is

$$\lambda_{max} = \frac{\boldsymbol{r_{max}}}{< \boldsymbol{r} >} = \frac{N\boldsymbol{b}}{\sqrt{N}\boldsymbol{b}} = \sqrt{N} \tag{2.7}$$

2.2.2 Neo-Hookean model

In continuum theory, the stress response of hyperelastic materials is derived from the given strain-energy function Ψ, and the neo-Hookean model is a special form of it. Before introducing the neo-Hookean model, I would like to take some time to introduce the Ogden model for incompressible materials.

The work is mainly done by Ogden [28,29,30]. The postulated stain energy is a function of the principal stretches λ_a, $a = 1,2,3$. It describes the changes of the principle stretches from the reference to the current configuration and has the form

$$\Psi = \Psi(\lambda_1, \lambda_2, \lambda_3) = \sum_{p=1}^{N} \frac{\mu_p}{\alpha_p} (\lambda_1^{\alpha_p} + \lambda_2^{\alpha_p} + \lambda_3^{\alpha_p} - 3) \tag{2.8}$$

where N is a positive integer which determines the number of terms in the strain-energy function, μ_p are constant shear moduli and α_p are dimensionless constants ($p = 1, \dots, N$).

The neo-Hookean model is derived from Eq.2.8 by setting $N = 1, \alpha_1 = 2$, using the first principle invariant $I_1 = tr\boldsymbol{b} = \lambda_1^2 + \lambda_2^2 + \lambda_3^2$, we have

$$\Psi = c_1(\lambda_1^2 + \lambda_2^2 + \lambda_3^2 - 3) = c_1(I_1 - 3) \tag{2.9}$$

where $c_1 = \mu_1/2 = nk_BT/2$.

Additionally, if we set $N = 2, \alpha_1 = 2, \alpha_2 = -2$, and use second principle invariant $I_2 = \frac{1}{2}(tr^2\boldsymbol{b} - tr\boldsymbol{b}^2)$, we can have Mooney-Rivlin model, which presents below as

$$\Psi = c_1(\lambda_1^2 + \lambda_2^2 + \lambda_3^2 - 3) + c_2(\lambda_1^{-2} + \lambda_2^{-2} + \lambda_3^{-2} - 3) \tag{2.10}$$
$$= c_1(I_1 - 3) + c_2(I_2 - 3)$$

where $c_1 = \mu_1/2\,, c_2 = -\mu_2/2$.

Fig.2-5 shows the comparison of neo-Hookean model and experimental data. In experimental data, we can witness a significant increase in nominal stress after a certain stretch. However, the neo-Hookean model fails to predict such change. It is only valid when the stretch is not high, which means the rubber does not undergo huge deformation, usually beyond 500% stretch.

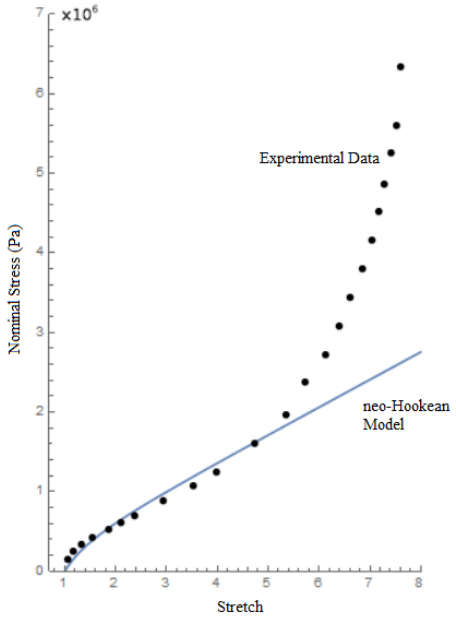

Fig.2-5. Curves of neo-Hookean model and experimental data

2.2.3 Arruda-Boyce model

In the experimental data, an increase in Young's modulus can be seen when the deformation is large. It is because the shear modulus μ varies with respect to deformation. To be more specific, μ decreases with increasing deformation at the beginning and then rises again significantly at large deformations [31]. In neo-Hookean model (Mooney-Rivlin model), we can obtain the shear modulus μ as $\mu = 2(c_1 + c_2) > 0$, which is a constant. Therefore, the neo-Hookean (Mooney-Rivlin) model is too simple for the characterization of the actual behavior of rubber.

The strain-energy function of Arruda-Boyce model is given as [32]:

$$\Psi = nk_B\theta\sqrt{N}\left[\beta\lambda_{chain} - \sqrt{N}\ln(\frac{\sinh\beta}{\beta})\right] \tag{2.11}$$

where N is the number of chain segments same as before, k_B is Boltzmann constant, n is the number of chains in the network of a cross-linked polymer.

$$\lambda_{chain} = \sqrt{\frac{I_1}{3}}, \qquad \beta = \mathcal{L}^{-1}\left(\frac{\lambda_{chain}}{\sqrt{N}}\right) \tag{2.12}$$

where I_1 is the first invariant of the left Cauchy–Green deformation tensor, and $\mathcal{L}^{-1}(x)$ is the inverse Langevin function which can be approximated by

$$\mathcal{L}^{-1}(x) = \begin{cases} 1.31\tan(1.59x) + 0.91x & for\ |x| < 0.841 \\ \dfrac{1}{sgn(x) - x} & for\ 0.841 \le |x| \le 1 \end{cases} \tag{2.13}$$

For small deformation, the Arruda-Boyce model reduces to neo-Hookean model, which experimentally verified by the collapse between the Arruda-Boyce curve and the neo-Hookean curve, as shown in Fig.2-6.

One alternative form of the Arruda-Boyce model by means of Taylor expansion is [33]:

$$\Psi = \mu\left[\frac{1}{2}(I_1 - 3) + \frac{1}{20n}(I_1^2 - 9) + \frac{11}{1150n^2}(I_1^3 - 27) + \frac{19}{7000n^3}(I_1^4 - 81) + \frac{519}{673750n^4}(I_1^5 - 243) + \cdots\right] \tag{2.14}$$

here we present first 5 terms for strain energy.

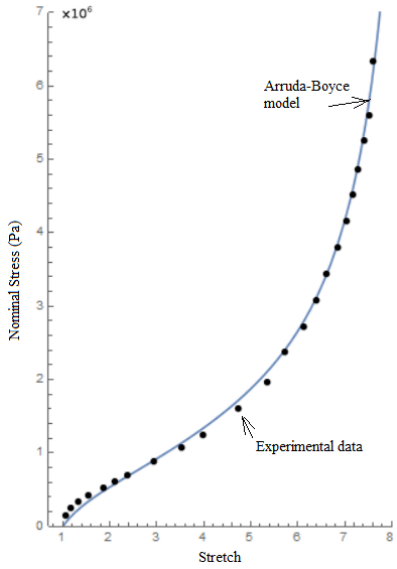

Fig.2-6. Curves of Arruda-Boyce model and experimental data

2.3 Viscoelasticity

As mentioned before, we took into account the viscoelasticity of the material we use to have a better replication of the real world. Here we are going to briefly introduce the viscoelasticity itself.

Viscoelasticity, as it can be conjectured from its name that it is the property of materials that exhibit both viscous and elastic characteristics when undergoing deformation. Viscous materials, like oil, resist shear flow and strain linearly with time when a stress is applied. Elastic materials strain when stretched and immediately return to their original state once the stress is removed,

which means no hysteresis occurs. Generally. The viscoelasticity can be separated as linear viscoelasticity and non-linear viscoelasticity. Linear viscoelasticity is usually applicable only for small deformations, while nonlinear viscoelasticity usually happens when the deformations are large or if the material changes its properties under deformations. Back to this thesis, the VHB tape we are using shows a non-linear viscoelastic behavior.

For linear viscoelasticity, if we use a dashpot to represent the viscous component and a spring to represent elastic component, then based on the foundation of the system, we may create the model of series connection (Maxwell model) and parallel connection (Kelvin-Voigt model). (Fig.2-7. a))

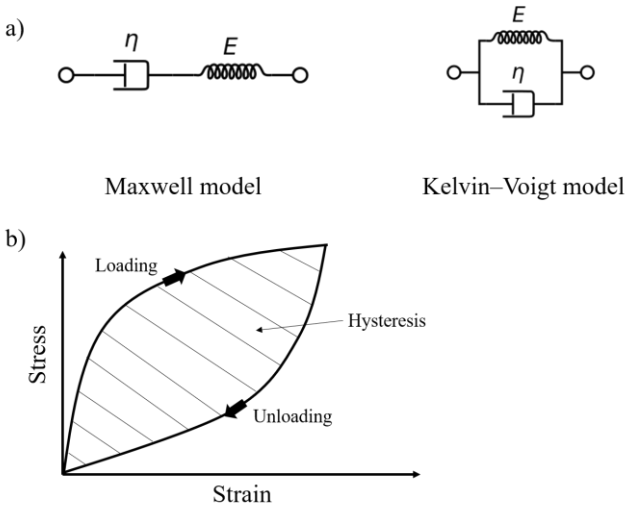

Fig.2-7. a) Maxwell model and Kelvin-Voigt model. b) Stress-strain curve

Due to the viscous component, the stress-strain curve of viscoelastic material always exhibits time-dependent strain. A typical curve of its stress-strain response is shown in Fig.2-7. b). A mathematical model is also listed below.

$$\sigma + \frac{\eta}{E}\dot{\sigma} = \eta\dot{\varepsilon} \qquad (Maxwell\ model)$$

$$\sigma = E\varepsilon + \eta\dot{\varepsilon} \qquad (Kelvin - Voigt\ model) \tag{2.15}$$

If we analyze the two models shown above, we can see that when the loading is very high at the very beginning, the strain rate will be zero, which means the material cannot deform under a sudden loading. However, some viscoelastic materials can deform at the start under fast loading. To compensate such scenario, people came up with standard linear solid model, which is also known as Zener model. A typical figure of such model is shown below and just like the regular viscoelastic model, it also has two representations.

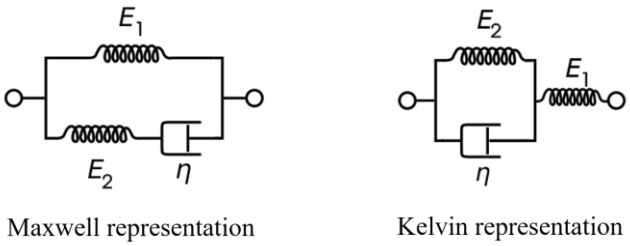

Fig.2-8. Standard linear solid model

For Maxwell representation, the mathematical model is

$$\sigma + \frac{\eta}{E_2}\dot{\sigma} = E_1\varepsilon + \frac{\eta(E_1 + E_2)}{E_2}\dot{\varepsilon} \tag{2.16}$$

And the mathematical model for Kelvin representation is

$$\sigma + \frac{\eta}{E_1 + E_2}\dot{\sigma} = \frac{E_1E_2}{E_1 + E_2}\varepsilon + \frac{E_1\eta}{E_1 + E_2}\dot{\varepsilon} \tag{2.17}$$

As the complexity of the material increases, the model becomes more and more sophisticated. Burgers model [34], generalized Maxwell model [35], etc. All of those are used in characterizing the materials in the real world.

It is also worth understanding the property from a molecular level. Since we have already talked about where the elastic property comes from in the previous section, here we will mostly discuss where the viscous component is from. One explanation is for the entangled polymers. Because the polymer chains are cross-linked, they may entangle with each other and create a mesh that is difficult for other polymer chains to go through. (Fig.2-9. c)) When the material is stretched, the friction between each polymer chain becomes into play and create lots of 'entanglement junctions'. Those junctions will be destroyed with the loading and the passage of time and the breaking of those friction junctions will create viscous response to the material. The friction model is also known as 'slip-link model'. (Fig.2-9. d))

Another explanation is for non-entangled polymers, which usually corresponds to dilute polymer solutions. The viscous part mostly comes from the interaction between the polymer molecules and the solvent molecules. Rouse model [36], which is shown in Fig.2-9. b), is one widely spread model that describes the viscoelastic behavior of short, linear chains in concentrated systems. It is derived from dumbbell model that pictures the polymer molecules as a dumbbell consisting two segments linked by a spring, (Fig.2-9. a)) and the dumbbell segments are surrounded by Newtonian fluid.

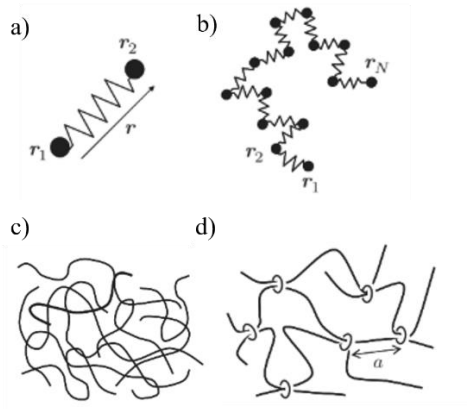

Fig.2-9. a) Dumbell model. b) Rouse model. c) Entangled polymer. d) Slip-link model. [27]

The derivation of mathematical model for entangled and non-entangled polymers can be found on articles [27,37,38]. Here we will skip the detailed derivation of such problems and use the literature above as reference.

2.4 Adhesion mechanics

We are examining the scenario of an adhesive membrane that peels off a rigid substrate, the scheme is in Fig.2-10.

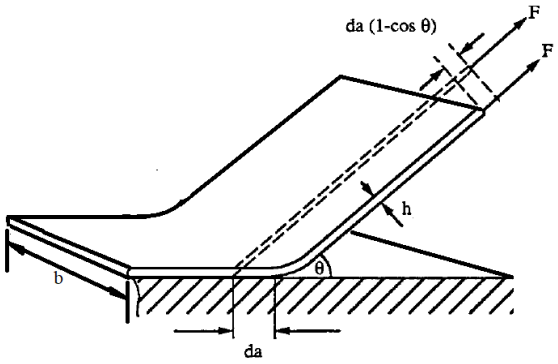

Fig.2-10. Peeling strip. Modified from Williams et al. [5]

In fracture mechanics, people use energy release rate to describe the energy dissipated during fracture per unit of newly created fracture surface area [39]. And the general definition of energy release rate G is described as:

$$G = \frac{d}{dA}[U_{ext} - U_s - U_d - U_k] \tag{2.18}$$

where U_{ext} is the external work; U_s is the strain energy; U_k is the kinetic energy; U_d is the dissipated energy and A is the area created.

If the strip is stretchable and has a small tensile strain ε, then the energy release rate may be written as:

$$G = \frac{F}{b}[1 - \cos\theta + \frac{1}{\sigma}\int_0^{\sigma} \varepsilon \, d\sigma] \tag{2.19}$$

In small deformation cases, the ε can be neglected hence the equation above will be simplified as $G = \frac{F}{b}[1 - \cos\theta]$.

To compute the peeling force of the thin membrane, we need can use the formula derived by Kendall [20].

$$P = \frac{b\gamma}{1 - \sin\theta} \tag{2.20}$$

where P is the peeling force and γ is the surface energy.

Another useful result is according to Williams et al, for an inflated two-dimensional bister (Fig.2-11), G and membrane force F can be computed as

$$G = pR(1 - \cos\theta) = pH$$
$$F = \sigma bh = bp\frac{a}{\sin\theta} = bpR \tag{2.21}$$

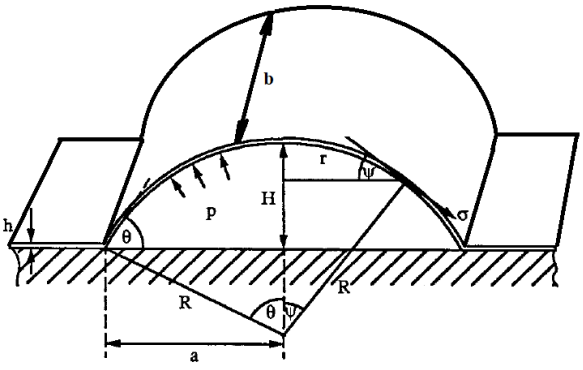

Fig.2-11. Inflated 2D blister

From Barquins et al. [40], and Barthel et al. [41], Chen et al. [47], gave us the result of crack speed as:

$$G(v_{crack}) = G_0[1 + (\frac{v_{crack}}{v_0})^n] \tag{2.22}$$

Form which, we can derive the Eq.2.28.

2.5 Inflating an air rubber balloon

The balloon instability is the crucial premise to understand the topic. Hence, we start with the simple scenario by analyzing the inflation of a rubber air balloon. The balloon is made out of rubber which is pure elastic and isotropic.

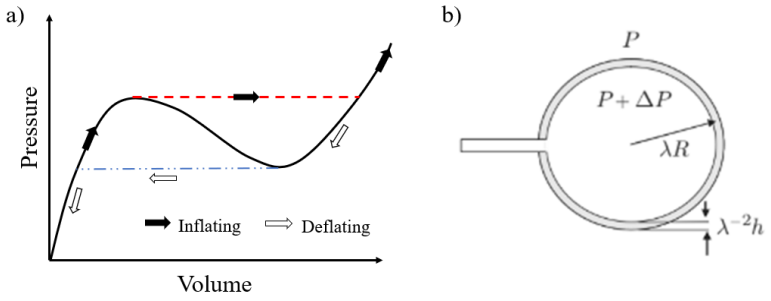

Fig.2-12. a) Pressure-volume curve of an inflating balloon. b) Balloon inflation problem

In this case, we study the pressure-volume curve of the inflated balloon, which is shown in Fig.2-12. a). As it is shown in the picture, the pressure inside the balloon experiences three stages throughout the inflation process. Let us assume the volume keeps increasing, the pressure first increases then decreases and finally increases again. In practice, it is easier to control pressure than volume, hence the inflation course will follow the solid arrow and the dashed line which will cause the volume to 'jump' to a larger value on the second ascending curve while maintaining the same pressure. Similarly, the deflating process follows the hollow arrow and the

double-dot dashed line and also experiences a 'jump' phenomenon. To better understand the whole transition, we need to combine it with Fig.2-6., which gives us the non-linearity of rubber material in general. Such behavior can be seen commonly when people are trying to blow up a rubber party balloon. The initial blowing procedure requires a strong effort followed by an easier inflating process, then the balloon becomes harder and harder to blow up until its rupture. How to understand such behavior is intriguing. Sophisticated mathematical methods are involved in the derivation of the pressure-volume curves [27,42]. One easy approach is through using free energy approach to derive, which is given by Masao, et al. (Fig.2-12. b)) Given that the rubber is incompressible, when in the one direction the rubber is stretched by λ in both θ (longitudinal) and ϕ (meridional) direction then it will be compressed by a factor of λ^{-2} in the other direction (radial). Given the free energy of deformation per unit volume is:

$$\Psi = \frac{\nu k_B T}{2}[tr(\boldsymbol{C}) - 3] \tag{2.23}$$

Given the deformation matrix $\boldsymbol{F} = \begin{bmatrix} \lambda & 0 & 0 \\ 0 & \lambda & 0 \\ 0 & 0 & \lambda^{-2} \end{bmatrix}$ and $\boldsymbol{C} = \boldsymbol{F}^T\boldsymbol{F}$,

Then here in this case we have:

$$\Psi = \frac{G}{2}(2\lambda^2 + \frac{1}{\lambda^4} - 3) \tag{2.24}$$

Then the total free energy of the system will be

$$F_{tot} = 4\pi R^2 h \frac{G}{2}\left(2\lambda^2 + \frac{1}{\lambda^4} - 3\right) - \frac{4}{3}\pi R^3 \Delta P(\lambda^3 - 1) \tag{2.25}$$

Where R is the radius of the balloon at force-free state, ΔP is the difference of the pressure in and out of the balloon. The second term represents the work needed to change the air volume in

the balloon ($W = \int_{V_0}^{V} PdV$). Based on the balance law, we set $\partial F_{tot}/\partial\lambda = 0$ to get the equilibrium state. Then we can obtain

$$\frac{R\Delta P}{Gh} = 2(\frac{1}{\lambda} - \frac{1}{\lambda^7}) \tag{2.26}$$

From which, we can have the pressure-stretch curve similar to Fig.2-9 but without the second uprising section. This explains why the pressure inside the balloon has a sudden drop when the volume reaches a certain point.

2.6 Inflation of a bubble on a rigid substrate

Here, we consider the membrane material to be hyperelastic, all of the analysis and results are based on such material property. Viscoelasticity is not applicable here.

a) Static analysis

To construct the model, we began with constructing an axisymmetric blister with volume V and neck radius R (Fig.2-13). For this, we parameterize the system by the arclength $\boldsymbol{s}$ and the revolution angle ϕ, and we consider its reference state, or original state, as a flat rubber disk of thickness h and radius R_0.

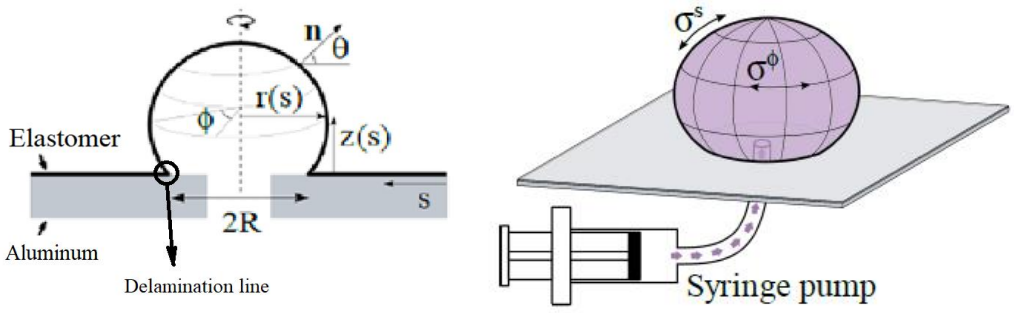

Fig.2-13. Scheme of an inflated blister

Regarding the material, the hyperelastic rubber is modeled using Arruda-Boyce model with Young's modulus E and chain link density N. Then, utilizing membrane theory in finite strain [46], we can determine the internal pressure of the blister, the longitudinal stress $\sigma^s(\boldsymbol{s})$ and meridional stress $\sigma^\phi(\boldsymbol{s})$ over the inflated area, and the geometry of blister. Nonetheless, our primary focus is on the adhesion mechanics of the rubber. As discussed before in Chapter 2.4, the adhesion energy (G) in thin shells ($R \gg h$) is well approximated by Eq.2.27(a):

$$G = \sigma^s(1 - cos\theta_d) \tag{2.27(a)}$$

where $\sigma^s(s_d)$ is the longitudinal stress at the delamination line, and $\theta_d(s_d)$ is the angle of the normal with the x-axis at that same location. However, in our analysis, this equation is not applicable because 1) it is derived from the scenario where there's no energy loss during the process. 2) It is only valid under small deformation. In one case we are examining, the membrane is viscoelastic, and the hysteresis of the material is not negligible. According to R. Long et al. [48], the energy release function can be described as Eq.2.27(b).

$$G = T_\xi^+(1 - cos\theta) + \frac{h_0}{\lambda_\xi^- \lambda_\phi}\left[\left.\frac{\partial W}{\partial \lambda_\xi}\right|_{\xi=\xi^+} \Delta\lambda_\xi - \Delta W\right] \tag{2.27(b)}$$

In which, the T_ξ^+ is the line tension in positive direction, h_0 is the thickness of the undeformed membrane. λ_ξ^- is the principle stretch where the contact edge is approached from negative ξ direction while the λ_ξ^+ is the principle stretch approached from positive ξ direction. Similar, the λ_ϕ is the principle stretch from ϕ direction. W is the strain energy function of the material that makes up the membrane.

The quantity of adhesion energy release rate relates to the work needed to detach a differential portion of the membrane, and it regulates its delamination process. In the real world, there is a

threshold value G_0, only above it will lead the tension inside the membrane high enough to break the adhesive bonds to delaminate it. By comparing this value with the intrinsic delamination threshold G_0, we can then divide each blister in two different categories: stable blisters ($G < G_0$) where delamination does not occur and unstable blisters ($G > G_0$) where delamination occurs. The delamination rate, which is characterized by the rate of changing radius, $\dot{R}$, is depicted by Eq.2.28:

$$\dot{R} = \begin{cases} 0 & if\ G < G_0 \\ v^*(\frac{G}{G_0} - 1)^{\frac{1}{n}} & if\ G \geq G_0 \end{cases} \tag{2.28}$$

where v^* is the critical velocity at which the effect of viscous dissipation at the crack tip becomes important, and n is known as the adhesion exponent and depends on the materials involved. In short, we can characterize the blister by the evolution of its delamination angle θ_L in time t, which is a function of the different parameters involved in the problem: $\theta_L = \theta_L\left(E, h, \dot{V}, v, G_0, L, t\right)$. In the meantime, only three dimensions (length, time and force) are involved in this problem, we can normalize the system in terms of 4 non-dimensional parameters, such that:

$$\theta_L = \theta_L(W, G^*, R^*, V^*) \tag{2.29}$$

The first parameter, $W = V/vh^2$, is a relation between the inflation and spreading dynamics, and it determines if this blister will grow in height (inflation prevails) or in width (delamination prevails). The second ($G^* = G_0/Eh$), third ($R^* = R/h$) and fourth ($V^* = V/h^3$) parameters correspond to the normalized delamination threshold, and respectively normalized volume.

Since the liquid filled in the blister is incompressible, the inflation mechanics can be understood in terms of V^*, R^* and G^*. Indeed, each pair of $V^* - R^*$ determines a unique blister profile (or

shape), whose stability inferred by its adhesion energy G^*. Moreover, due to the definition of G (Eq.2.27(b)), G^* shows similar nonlinear behavior to the pressure and its variation within the $V^* - R^*$ space results in the surface of Fig.2-14. With the help of such surface, we can define a phase diagram by looking at the intersection between the surface and the plane $G^* = G_0$. For most cases, it will intersect the plane with up to four different stability regions indicating whether each pair of $V^* - R^*$ is stable (with no delamination occurs) or unstable (with delamination occurs).

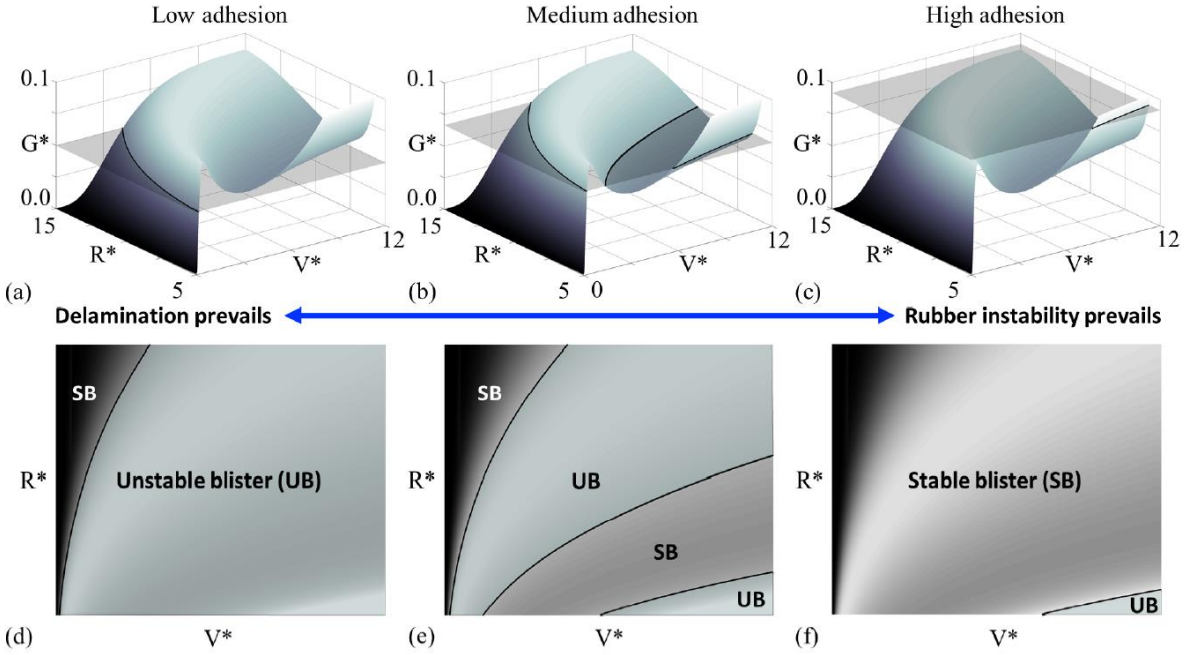

Fig.2-14. Top: Variation of the adhesion energy G^* versus the normalized neck radius R^* and volume V^*. A plane at constant G^* cuts teach surface at different points corresponding to (a) $G^* = 0.06$, (b) 0.08, and (c) 0.11. Bottom: Phase diagram $V^* - R^*$ where the lines (corresponding to the intersection of the plane above) delimit the stabile (no-delamination) and unstable (delamination) regions.

The phase graph is useful that can help us understand the process of a blister when being inflated. For example, starting from a blister at zero volume ($V^* = 0$), we first encounter a stable region corresponding to the initial inflation until G_0 is reached for the first time. As the volume increases, the blister enters an unstable region and most noticeably, this region is where delamination occurs according to Eq.2.28. The third state is a consequence of the non-linearity of the pressure (and G by extension). Fig.2-15. shows the non-linearity of the pressure when a rubber-like blister is inflated and the whole process is depicted in Section 2.5.

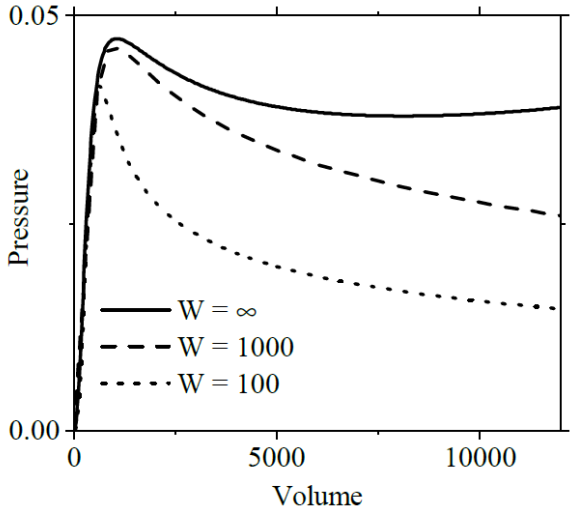

Fig.2-15. Non-linearity of the pressure when rubber blister is inflated

In the third state, an additional stability regime might exist at higher volumes if G drops below the delamination threshold (G_0) again. In other words, the blister is 'trapped' (no delamination) even having a higher liquid volume. The fourth region happens based on the stiffening feature of the rubber material, will inevitably leads to a final instability where the blister delaminates.

However, determined by the initial adhesion G_0, not all systems show these four distinct states. With the very low adhesion, the blister will reach the onset of delamination at very low volumes and the energy drop du to the rubber non-linearity is not enough to reach the second stable state.

Therefore, the mechanics are dominated by the adhesive instability. On the contrary, situations with super high adhesion will lead to blisters that do not delaminate until the material is highly stiffened (assume the material will never reach its failure stress). The mechanics here are mostly driven by the rubber instability.

b) Dynamic analysis

According to the previous static analysis, we showed that the phase diagram of Fig.2-14 allows a stability classification of any blister defined by a pair $V^* - R^*$. However, during the experiments, we found that this information is not sufficient to establish its inflation history which depends on the non-dimensional spreading coefficient W. The fact is, due to the existence of different stability regions at the same volume (Fig.2-14), a fast inflation of a blister might lead to a different stable state than a slow one.

To better comprehend this process, we consider the motion of a blister in the $V^* - R^*$ plane as:

$$\dot{x} = \begin{Bmatrix} \dot{R} \\ \dot{V} \end{Bmatrix} = \begin{Bmatrix} \dot{R}(W, R^*, G^*) \\ v^* h^2 W \end{Bmatrix} \tag{2.30}$$

where $\dot{R}$ is given by Eq.2.28. This system of differential equations can be directly integrated in cases where there is no inflation ($\dot{V} = 0$), or no delamination ($G < G_0, \dot{R} = 0$). Otherwise, we must consider the relationship between the delamination velocity and the volume as $\dot{R} = \frac{dR}{dV}\dot{V}$. Substituting $\dot{V} = Wh^2 v^*$ and Eq.2.28, this leads to the following differential equation that governs the dynamics of blister growth when inflation and delamination coexist:

$$W\frac{dR}{dV} = \frac{1}{h^2}\left(\frac{G}{G_0} - 1\right)^{\frac{1}{n}} \tag{2.31}$$

and which can be numerically integrated given the initial volume (V_0^*), neck (R_0^*) and spreading coefficient W. This solution enables determining the evolution of the blister in time and consequently predict its behavior depending on the initial conditions. Hence, we can establish two different dynamic situations for each blister in the plane $V^* - R^*$. When the blister inflation occurs on the stable region ($G^* < G_0^*$), there is no delamination and the blister grow at constant R following a horizontal path in the phase diagram. Alternatively, if the blister is located in the unstable region ($G^* > G_0^*$) delamination occurs and the blister neck grows at a rate depending on W, i.e. $v = v^*(\frac{G}{G_0} - 1)^{\frac{1}{n}}$

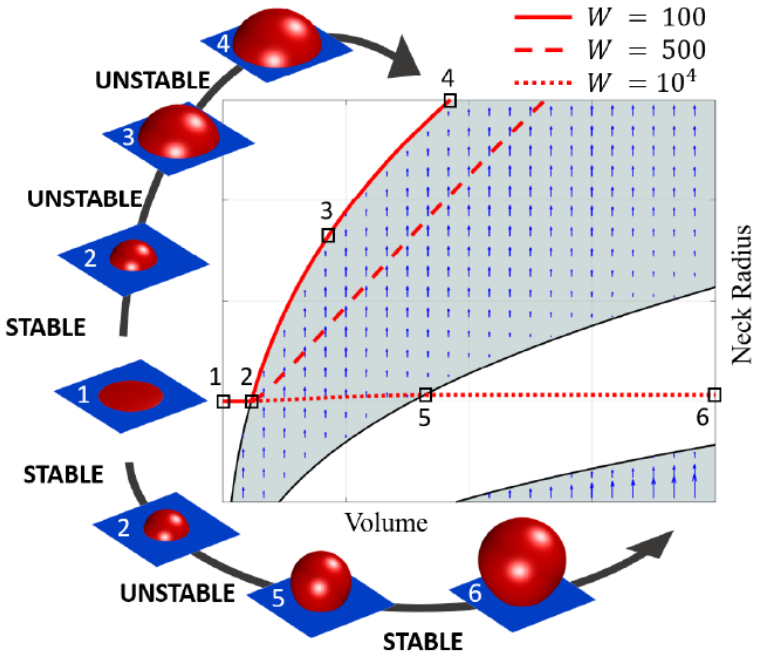

Fig.2-16. Dynamic instability of blister

Let us use an example to better show this process. Consider three different cases in which an initially flat blister $V(t = 0) = 0$ is inflated at different rates such that $W = 100,500,10000$ (Fig.2-16). Initially, all blisters follow the same path (1-2). Since the pressure is low, there is no

delamination, and the blisters go through the same growth process at different speeds. However, once we reach point 2, delamination starts to occur, and three paths start to diverge.

In the case of slow inflation ($W = 100$), the dynamics of delamination are much faster than the inflation rate. Indeed, as G approaches zero, we can establish $dG \to 0$, such that $\frac{dG}{dR}\dot{l} + \frac{dG}{dV}\dot{V} \to 0$, or equivalently $\dot{R} \to Wh^2v^* \frac{-dG/dR}{dG/dR}$, so we obtain that $\dot{\boldsymbol{x}} = Wh^2v^* \frac{dG}{dR}\begin{Bmatrix} -dG/dV \\ dG/dR \end{Bmatrix}$, such that the blister follows a line tangent to the intersection between the 3D surface and the plane $G = G_0$. In other words, the blister follows a quasi-static growth going through the limiting curve between stability and instability (2-4). On the intermediate inflation ($W = 500$), there is a competition between the delamination and volumetric growth. However, as long as the blister remains on the unstable regime, its final state will be the same as a slowly inflated blister of equal volume. Finally, in the fast inflation case ($W = 10000$), the volumetric growth dominates over delamination, and the blister neck barely changes during the inflation process. Therefore, the blister follows an almost horizontal path (2-6) such that it is able to bypass the unstable region and reach the second stability regime. At this point, the blister continues to grow, but its neck does not, which means it is trapped. This situation, however, does not extend forever and it reverses when the material enters a stiffening regime as the tension increases again.

Chapter 3

Experimental Results

3.1 Methods of materials for EcoFlex™ 00-30

3.1.1 Experiment preparation

To begin with, we examined the widely used rubber Ecoflex™ 00-30, it is a type of widely used silicon rubber both in daily life and in academia.

In order to test the theory, we built our own experimental system. It contains a substrate made of aluminum, a rubber (elastomer) membrane, a syringe and a syringe pump, a DC power source, a pressure transducer, and a data acquisition system (DAQ). In the meantime, wires are used as digital signal transmitters and polyethylene tubing is used as water path. Table 3.1 lists all the components of the system, while the scheme of the entire system is in Fig.3-1.

Table 3.1: Inventory of experiment system for EcoFlex™ 00-30

Item	*Material & Specification*	*Quantity*
Substrate	Aluminum board	1
Membrane	EcoFlex™ 00-30 (A:B=1:8) Curing in oven at 60°C, 1h	Thickness dependent
Thickness control	Aluminum tape: Nashua 324A, 0.1mm/layer for EcoFlex™	Thickness dependent
Water path	BTPE-90 Polyethylene tubing	2
Syringe	HSW Norm-ject 50mL	1
Syringe pump	NEWERA Pump Systems Inc. NE-300	1
Pressure transducer	Omega PX26-005GV	1

DAQ system	NI-DAQ 9211A + NI-USB 9162 Carrier + 198506D-01 USB Cable	1
DC power source	LONGWEI® LW-3010KDS	1
Software	LabVIEW 2016/2017	1
Others	J-B WELD ClearWeld Epoxy, paper cup, glass stir, hole cutter	

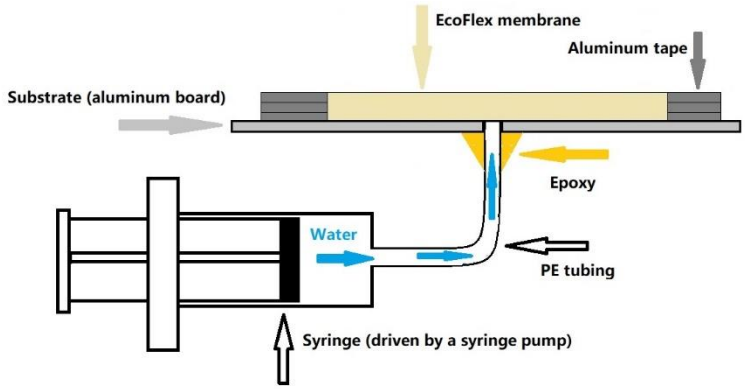

Fig.3-1. Scheme of the blister testing setup for EcoFlex^{TM} 00-30

To simplify the blister structure, we consider the blister as a membrane attached to a substrate, while the forming of the blister is induced by pumping water between the substrate and the membrane through an existing hole. Scheme and actual picture are shown in Fig.3-2. We use Nashua 324A aluminum tape to form a mold for the membrane. Additionally, it will be served as a thickness control agent of the membrane by piling up the aluminum tape with 2-inch diameter holes to the exact height that we want. From measurement, we know that each layer of aluminum tape is 0.1mm, which means if we want the thickness to be 0.5mm, then we need to put 5 layers of aluminum tape. Holes on the tape are made by a precise hole puncher. The substrate is made of an aluminum board, we cut it into smaller pieces and drill a hole on each individual one. The drilled hole is in 1/16-inch diameter.

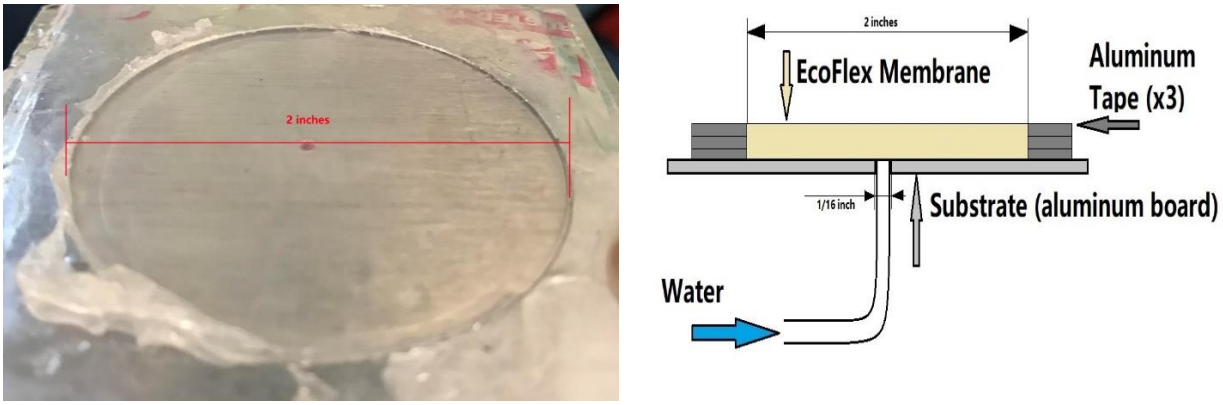

Fig.3-2. Blister testing structure

The main component is the EcoFlex™ membrane. EcoFlex™ rubbers are platinum-catalyzed silicones that are made by mixing its part A and part B with a specific ratio by weight or by volume. Here we use EcoFlex™ 00-30 silicon rubber with the ratio of part A and part B is 1:8, which will provide us a desired stiffness of membrane. The fabrication procedure of the blister testing device is as follows. Firstly, prepare a 2-inch long PE tubing, fill it with epoxy, attach the tubing to the 1/16-inch hole from the other side of the substrate using epoxy, make sure the tip of tubing is at the same height as the top surface of the substrate, put the entire setup on a horizontal surface, wait until epoxy cures. In this case, we can prevent EcoFlex™ from leaking through the 1/16-inch hole. Secondly, we prepare proper amount of EcoFlex™ part A and part B, mix them together thoroughly to form a prepolymer. Thirdly, we pour the prepolymer into the aluminum tape mold, use a glass slide to scrape off the extra liquid, make sure the top of the liquid and the top of the mold are on the same level. Wait 10 minutes to let the bubble inside to escape. Then we put the setup in the 60° C oven until the prepolymer cures. Once the previous steps are done, we take the setup out of the oven using tweezers and pull the tubing out of the epoxy carefully without damaging the membrane. Here we have a blister testing device. Finally, we attach another tubing, which has already been connected to the syringe and filled with water, to the

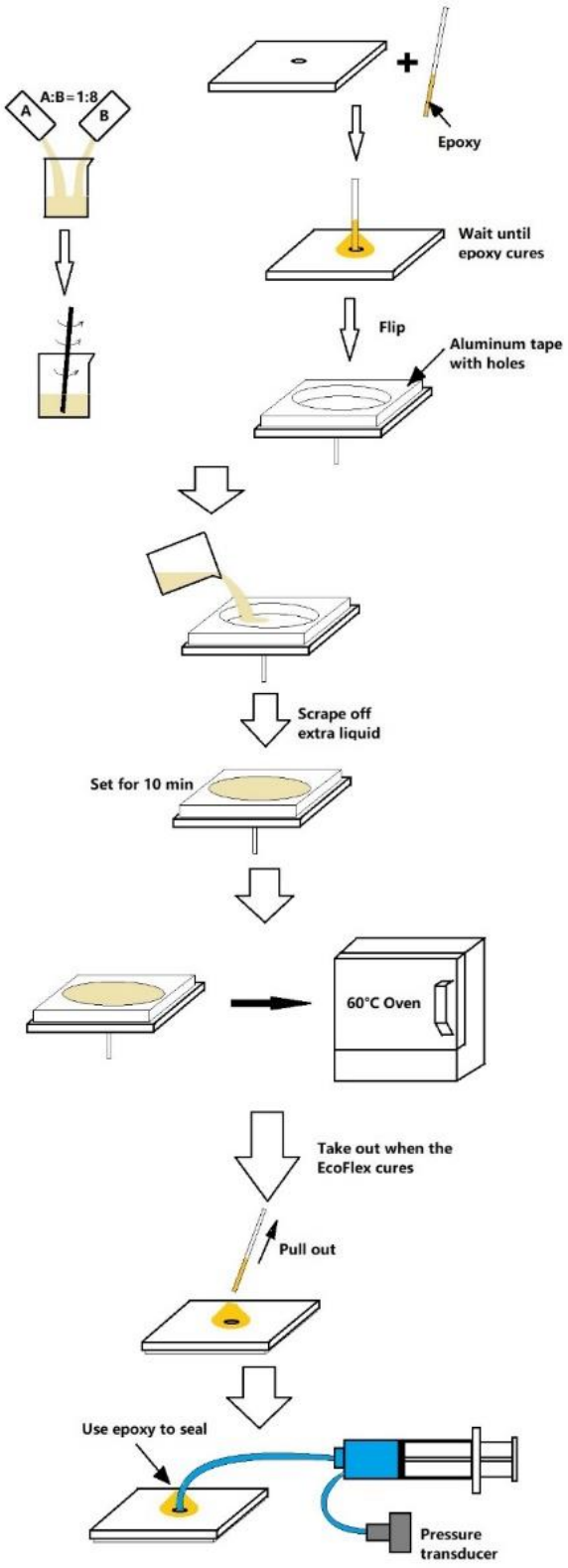

Fig.3-3. Scheme of EcoFlex^{TM} 00-30 experiment preparation

1/16-inch hole through the existing epoxy and use new epoxy to seal the leakage. Wait until new epoxy cures, the whole system is set. The schematic of the procedure is depicted in Fig.3-3.

3.1.2 Conducting experiment

Having the device, we can conduct the experiment. Firstly, we want to eliminate the influence of water, so the blister test device should be submerged in water. For data gathering, we use 2 cameras to capture the graph from both the top and the side. By taking the pictures at the rate of 1 picture per second, we can track the changes of its radius using ImageJ software. Another set of data is pressure-volume data. The volume rate is manually set by the experimenter on NEWERA Pump Systems Inc. NE-300 syringe pump. To gather pressure data, we are using Omega PX26-005GV pressure transducer, it is a low-cost pressure transducer when powered with 10 V, measures 10 mV per psi up to 5 psi. It transforms pressure information into voltage information. The transformation equation is listed below.

$$P = 0.689476V \tag{3.1}$$

Here, P is pressure (kPa), V is the voltage read by DAQ system (mV).

To read the measurement, we use NI DAQ system (NI-9211 and NI USB-9162) along with LabVIEW software. Using the equation above we can obtain the pressure information. The whole setup is in Fig.3-4.

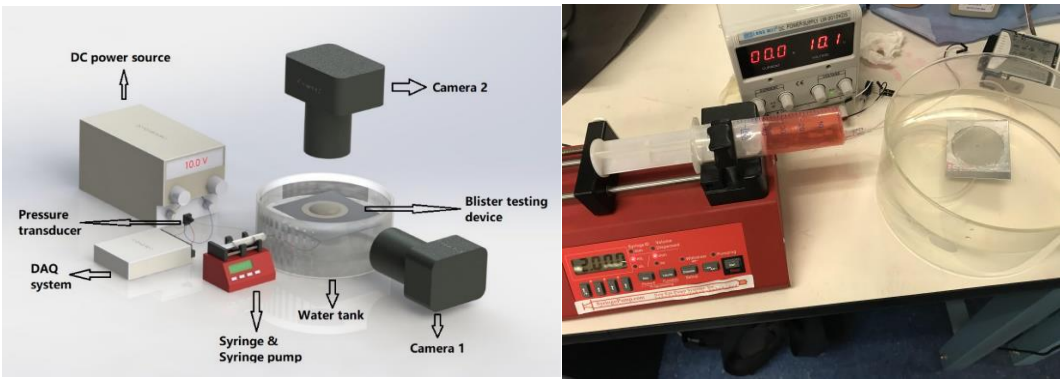

Fig.3-4. Scheme and the real picture of the system

Having the pressure, we also need the data of the blisters' profile. Here we use SONY α 200 camera to capture the profile data, basically taking pictures sideways and use ImageJ software to measure the neck radius R. The data will be processed by using Microsoft Excel 365 and MATLAB 2017b.

3.1.3 EcoFlex™ results

a) Tensile test

Even though the overall mechanical property of EcoFlex™ is well studied both by the company and by researchers, some still remain to be discovered. For instance, the recommended way of using EcoFlex™ is to mix the part A and part B with the ratio of 1:1. However, we did several preliminary tests of different mixing ratio and found that the 1:8 (part A : Part B) ratio can give us maximum adhesion while maintaining its shape. For higher ratio (more part B with respect to part A), the rubber can not cure under every circumstance. Since no study has ever done on EcoFlex™ at 1:8 ratio, we need to examine its basic mechanical properties, which, in our case, is its stress-strain response.

The tensile test is done on the INSTRON machine. To prepare the tensile test, we need to prepare samples with a special shape ‘dog bone’. Fig.3-5. shows its actual shape and how it is installed on the machine.

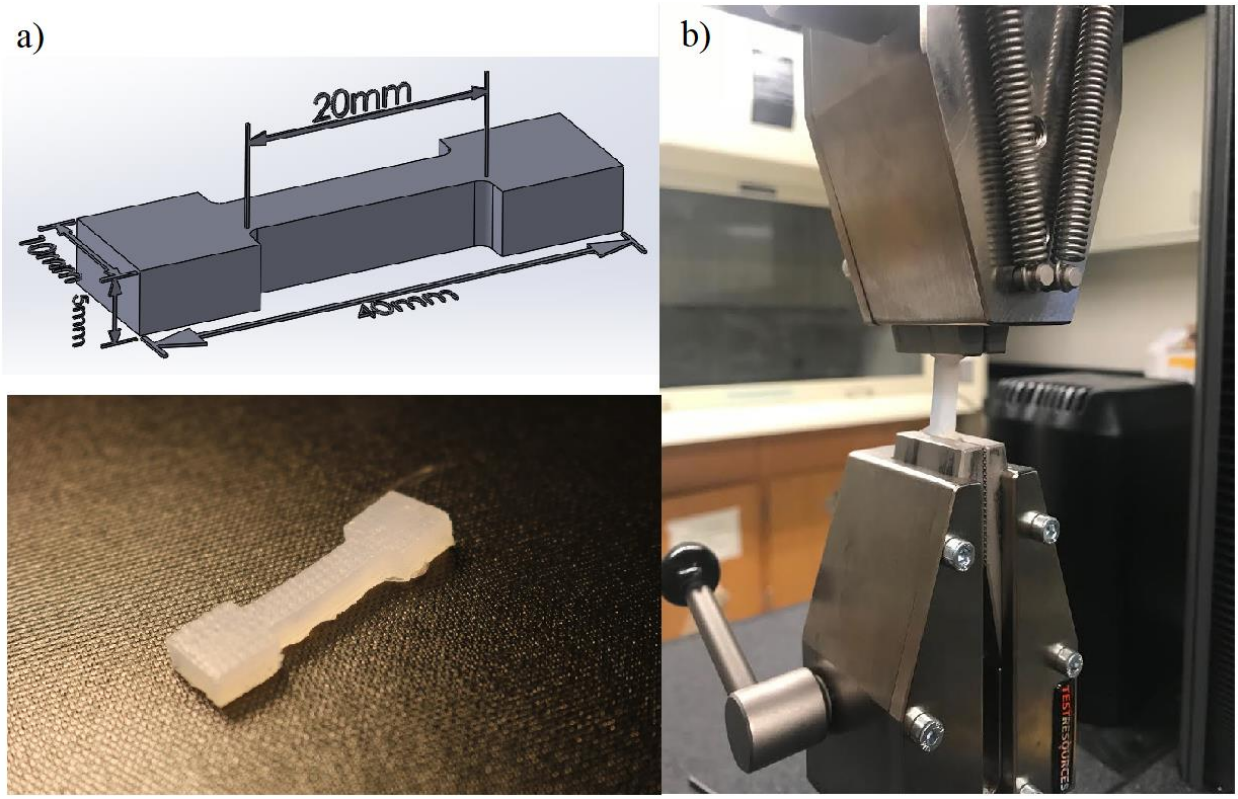

Fig.3-5. a) The dimension and photo of a sample. b) Sample on INSTRON machine

The loading rate we used was 50%/min. One good aspect about EcoFlex^{TM} is that it is hyperelastic, with no factor of viscosity. Fig. shows the tensile test result of EcoFlex^{TM} 00-30 with the mixing ratio of A : B=1 : 8. Note: the material failed at the stretch of approximately 640%.

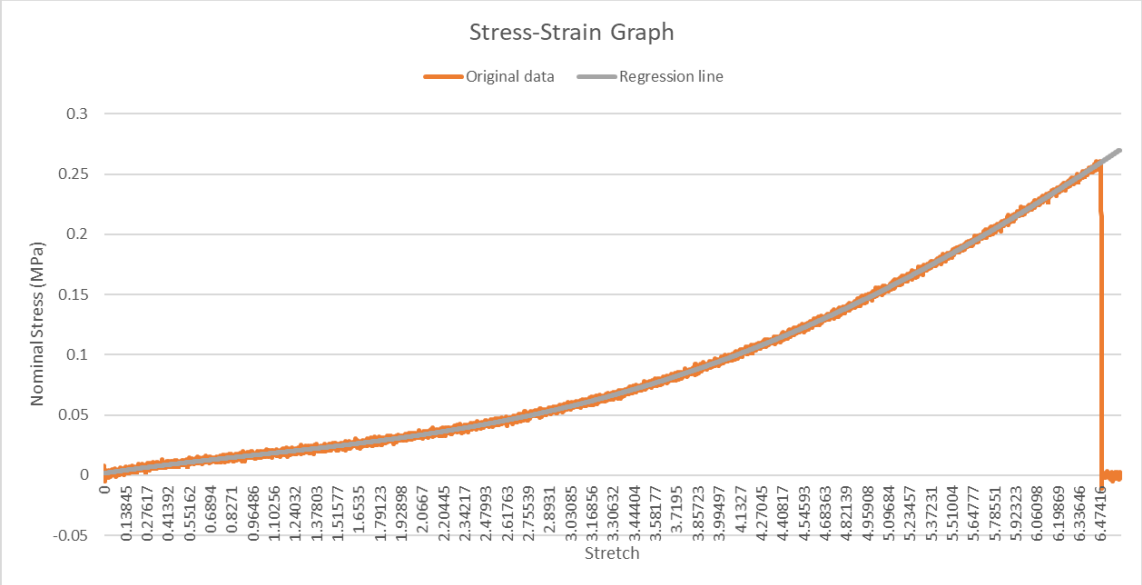

Fig.3-6. One result of the tensile test for EcoFlex^{TM} 00-30 with mixing ratio of A:B=1:8

To obtain Young's modulus E, we need to use the formula of neo-Hookean material.

$$\boldsymbol{\sigma = G\left(\lambda - \frac{1}{\lambda^2}\right) = \frac{E}{3}\left(\lambda - \frac{1}{\lambda^2}\right)} \tag{2.11}$$

This is the constitutive equation for elastomeric material, where σ is the stress, λ is the strain, E is the Young's modulus remains to be fitted. Fig. shows the fitting result. Since the equation is based on the neo-Hookean model, it does not have the feature of stiffening, while the experimental result has. From which, we can get the Young's Modulus as $E = 0.03MPa$.

We also used the Arruda-Boyce model to fit the material and the result is in Fig.3-8. The average of Young's modulus $E = 0.029MPa$, which is really close to what we get using neo-Hookean model, with the standard deviation of 0.0028 and the N value is 1.66 with the standard deviation of 0.0561.

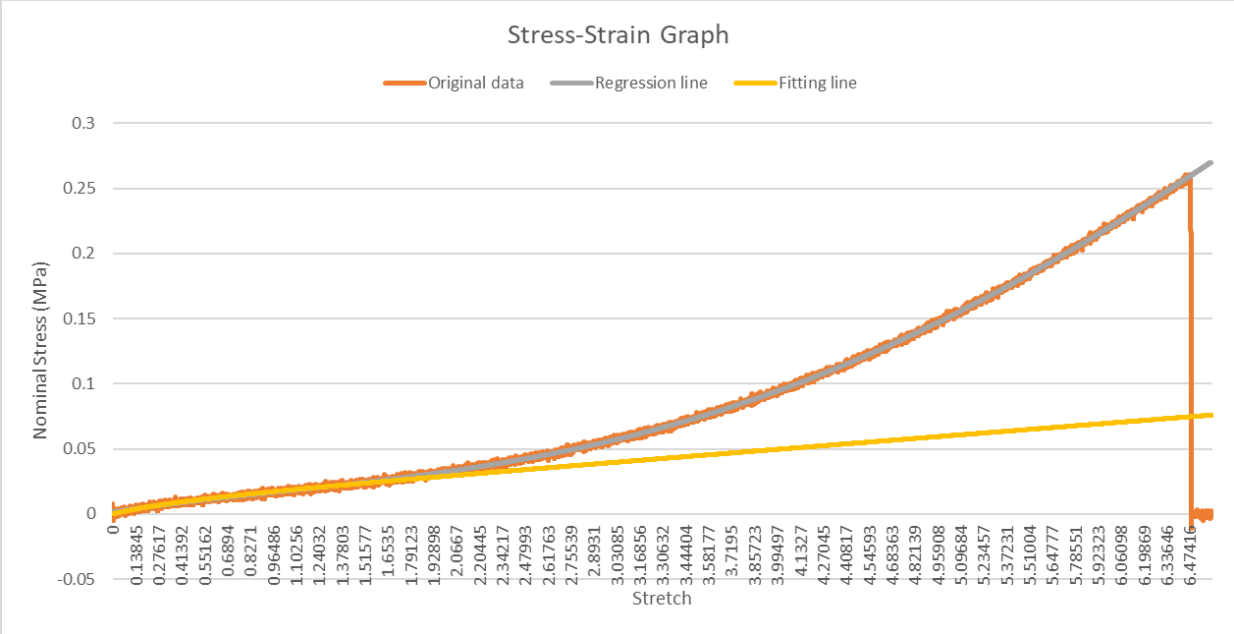

Fig.3-7. Fitting result of $E = 0.03MPa$

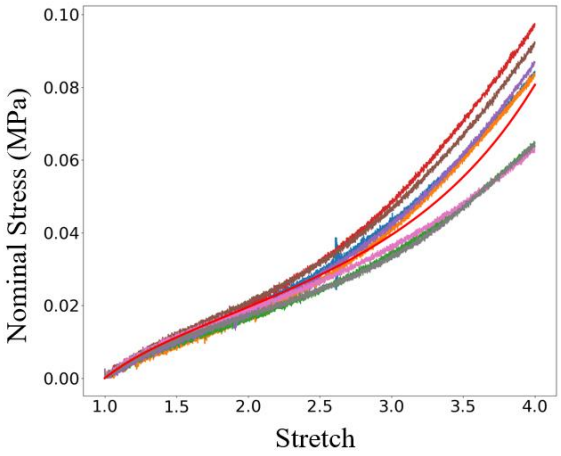

Fig.3-8. Fitting result using Arruda-Boyce model

b) Initial results

Even though the EcoFlex™ is slightly viscoelastic, the result for EcoFlex™ blister testing is quite unsatisfying. Mostly because the material (EcoFlex™ 00-30 1:8 mixing ratio) does not have a great mechanical property. The original EcoFlex™ 00-30 with the mixing rate of 1:1 can

not give us a good adhesion to the substrate while the mixing ratio 1:8 cannot give us a desired strength of the membrane. Another drawback is that the low mixing ratio will create a low N in Arruda-Boyce model. The low N value will promote the stiffening point to a very early stage. The pressure-volume data is shown in Fig.3-9. To get this data, we use a ring with a radius of 3.5mm to regulate the delamination and the thickness is 0.35mm. While the inflation rate is 0.5mL/min. Ideally, the constrained pressure value should go below the G_0 value to reach the stable region just like Fig.2-15. But in this situation, the pressure value keeps going up. On the one hand, this phenomenon proves that the material is very easy to become stiffen, on the other hand, it shows that this blister can never be trapped, which means it will never go to the stable region. In the delamination curve (dash line), the pressure will eventually drop to some point close to the beginning pressure because of the material stiffening. Therefore, this material is not good enough to study the instability of blister. However, we still get some preliminary validated data towards our goal.

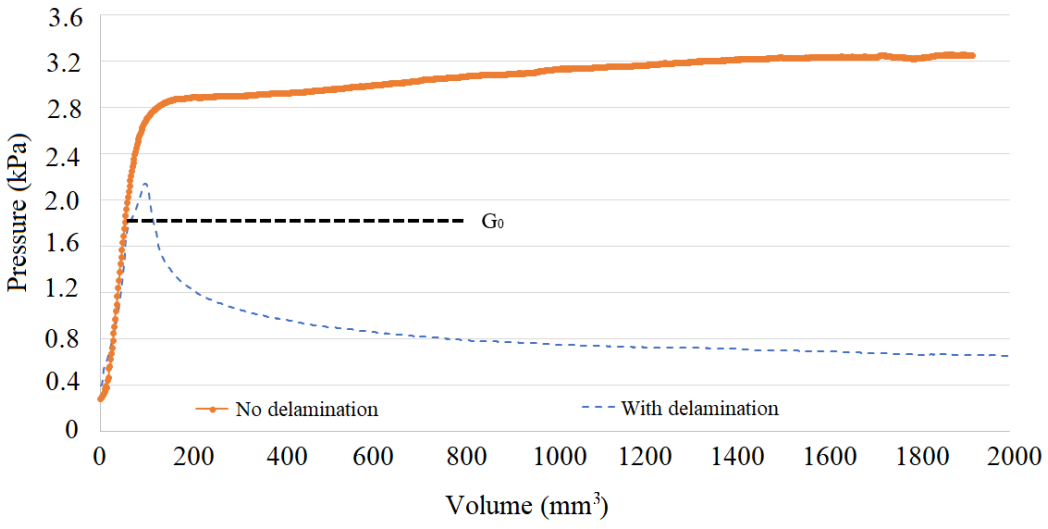

Fig.3-9. Delamination and non-delamination curve of EcoFlex™ 00-30

One thing we first examine is how the pressure changes when the inflation rate changes. In the theory, as the inflation rate increases, the maximum pressure inside the blister should not increase due to the pure elastic property of the material. However, when we change the inflation rate from 0.5mL/min to 4mL/min while maintaining the initial radius constant and the thickness of the membrane as 1.05mm (9 layers of aluminum tape), we find that the result is shown in Fig.3-10 and the maximum pressure is different. According to this result, we can tell the 1:8 mixing ratio of EcoFlex could be viscoelastic. In the meantime, because of the defect that could induce the difference among different experiments, for example, the thickness may be different, or the initial detachment could be various too. This may cause the result to vary a lot.

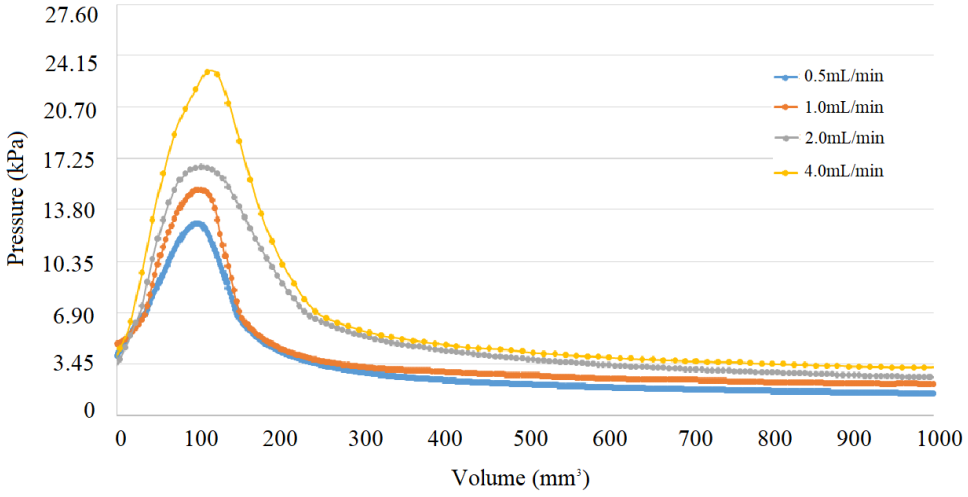

Fig.3-10. Pressure-volume data for different inflation speed

Another feature we examined is the influence of the thickness. Since the EcoFlex™ is relatively easy to change the thickness as we wish, we believe it is quite good to show the thickness factor. Here, we choose to use 3 layers, 9 layers and 12 layers of aluminum tape to set the thickness difference. The inflation rate is 1mL/min. The results are shown in Fig.3-11. From which, we can make a conclusion that under the same inflation rate and same material (which means same

Young's modulus and same adhesion to the same substrate), the thicker the membrane is, the higher the pressure in the blister will be.

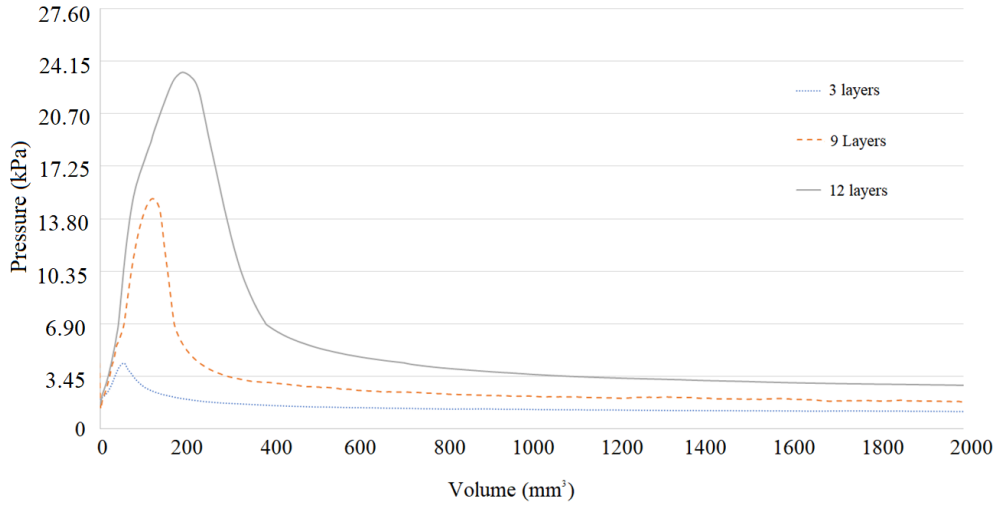

Fig.3-11. Pressure-volume data for different membrane thickness

In conclusion, even though the result for the EcoFlex^{TM} 00-30 at the mixing ratio of 1:8 is not satisfying, they do give us a preliminary understanding of the problem and allow us to test the basic validity of our theory. We need to find another material which should be hyperelastic that is good enough to test our theory of the pure elastic case.

3.2 Methods of materials for 3M^{TM} VHB tape

3.2.1 Experiment preparation

Our next goal is to study how the viscoelasticity involves in the scenario. Therefore, we choose to use the 3M^{TM} VHB tape as our sample material. It is widely used as a heavy-duty adhesive in engineering purposes, like gluing the glass on the wall, or attach a transparent protective screen on cars' windshields. But in academia, it is also widely used in soft actuators and soft electronics. Because of its dielectric property, it is widely used in artificial muscle structures.

3M™ VHB Tapes are a family of double-sided foam tapes made from high-performance acrylic adhesives. These tapes are able to form bonds of exceptional strength while maintaining durability and elasticity. All 3M™ VHB Tapes use closed cell technology and provide outstanding environmental resistance and durability [43]. The good side of VHB tape is that it is produced through industrial processes, so the quality of the tape is quite unique, unlike the Ecoflex™ whose mechanical property may vary from patch to patch.

The setup we designed for the 3M™ VHB tape is similar to what is used in EcoFlex™ test. It also contains a substrate made of aluminum (the reason we choose aluminum is based on the manual provided by 3M™ company, saying that the adhesion between VHB tape and aluminum is categorized as super strong [44]), VHB tape, a syringe and a syringe pump, a DC power source, a pressure transducer, a DAQ system, wires and tubes. Since the thickness of VHB tape is predefined, we do not need to worry about its thickness. Table 3.2 lists all the components of the system, while the scheme of the entire system is in Fig.3-12.

Table 3.2: Inventory of the experiment system for VHB tape

Item	*Material & Specification*	*Quantity*
Substrate	Aluminum board	1
Membrane	3M™ VHB tape	1
Water path	BTPE-90 Polyethylene tubing	2
Syringe	HSW Norm-ject 50mL	1
Syringe pump	NEWERA Pump Systems Inc. NE-300	1
Pressure transducer	Omega PX26-005GV	1
DAQ system	NI-DAQ 9211A + NI-USB 9162 Carrier + 198506D-01 USB Cable	1
DC power source	LONGWEI® LW-3010KDS	1

Software	LabVIEW 2016/2017	1
Others	J-B WELD ClearWeld Epoxy, Hole cutter	

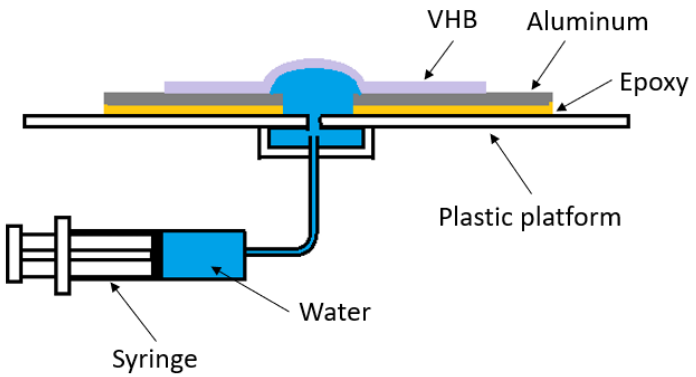

Fig.3-12. Scheme of the blister testing setup for VHB tape

We have already introduced the sample preparation procedure of EcoFlex™. On the contrary, the sample preparation here is quite simpler. Firstly, we need to fill the channel with water all the way to the top surface of the aluminum board. After we make sure there is no air trapped in the system, we take a slice of VHB tape and carefully attach it to the top surface and seal the hole. The VHB tape, which has two sticky sides, usually has one side covered with a red plastic protection layer. When the VHB tape is attached to the aluminum surface, we use the sticky side and leave the protection layer on. We let the VHB rest on the surface for more than one hour to increase the adhesion. If stronger adhesion is needed, we can use the oven to heat it up according to the user manual [44].

Then, we can peel off the protective layer and, if needed, we can attach a constraint layer to create a non-delaminated neck for the blister. The whole process is shown in Fig.3-13.

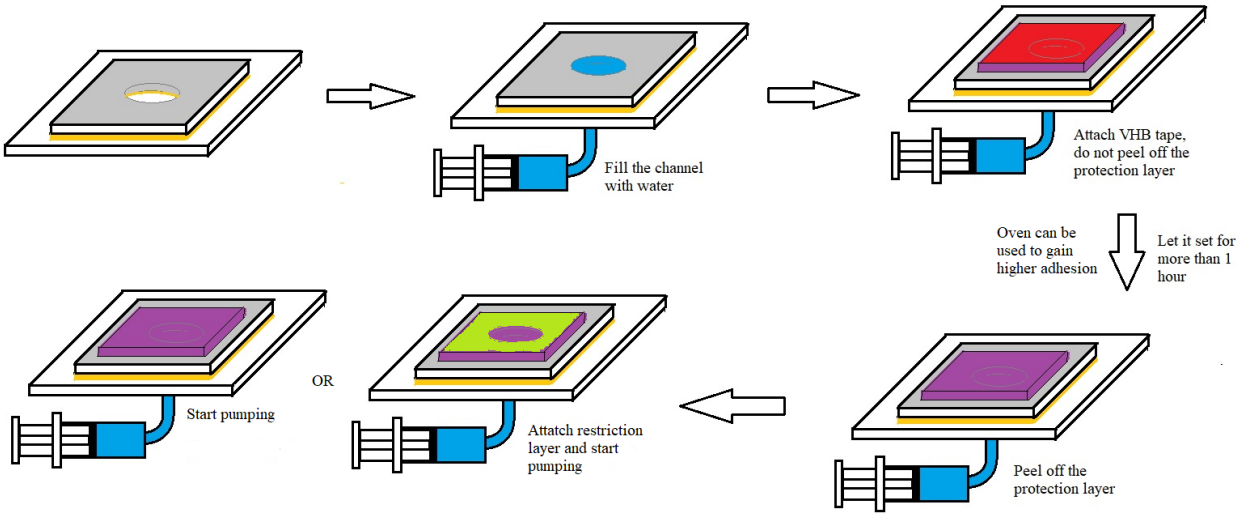

Fig.3-13. VHB tape sample preparation

3.2.2 Conducting experiment

Based on previous sample preparation, we can conduct the experiment. The experimental setup is similar to the previously used setup for EcoFlex™, with minor changes to accommodate new features. Here we designed a new supporting structure. Since water may dissolve the adhesion and we couldn't determine to what extent it may influence our result. In this scenario, we didn't use water to gain a more consistent result. The picture of the whole system is shown in Fig.3-14.

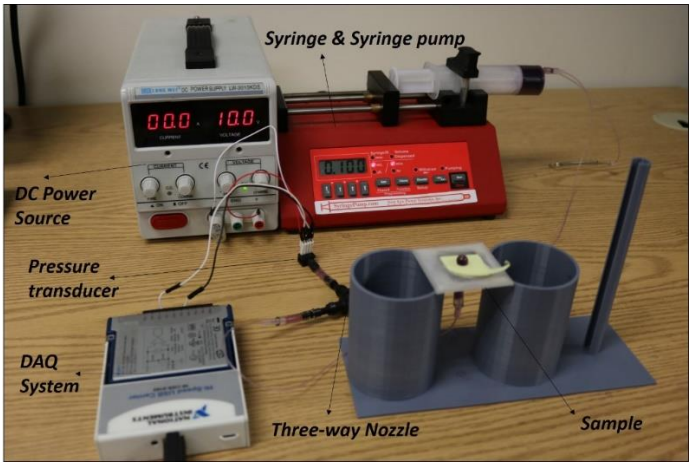

Fig.3-14. Picture of the testing system for VHB tape

The data gathering process is the same as the process used for EcoFlex™ tests. The DAQ system records the pressure data and 2 cameras record the picture data. The syringe pump can provide the data for the volume and the inflation rate.

3.2.3 3MTM VHB tape results

a) Viscoelasticity

To know better about the material, we conducted the uniaxial tensile test using INSTRON machine. The sample we use is 3M™ VHB 4905 tape, with a thickness of 0.5mm and width of 12.7mm. In this method, we found that the material undergoes significant shrink at the center of the sample. To have a better result, we use the camera to capture the distance between markers on the sample to get the accurate stretch. Fig.3-15 shows a series of the pictures we take, and we measure the distance between two lines using ImageJ software. The number on the sample is the initial distance (mm) before the sample is stretched.

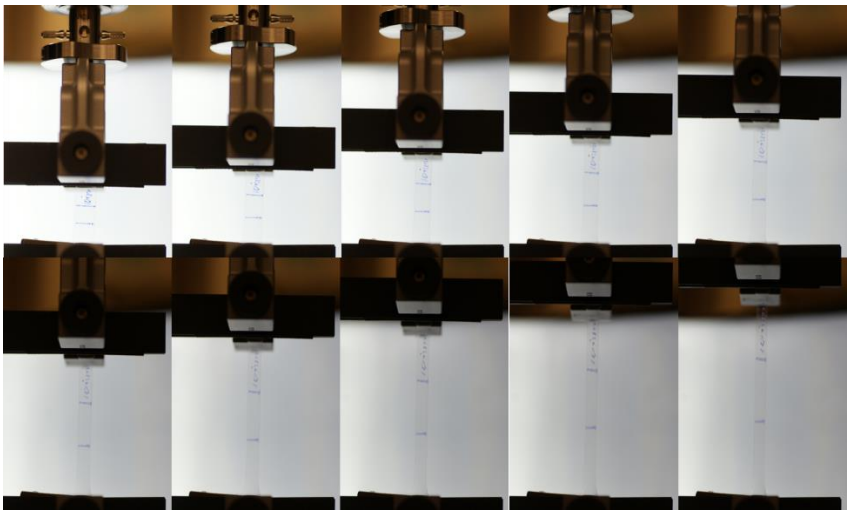

Fig.3-15. Uniaxial tensile test

Fig.3-16 shows the results. As is shown in the figure, under different loading rate, the material has a different stress-strain response, which can be understood as the result of viscoelasticity.

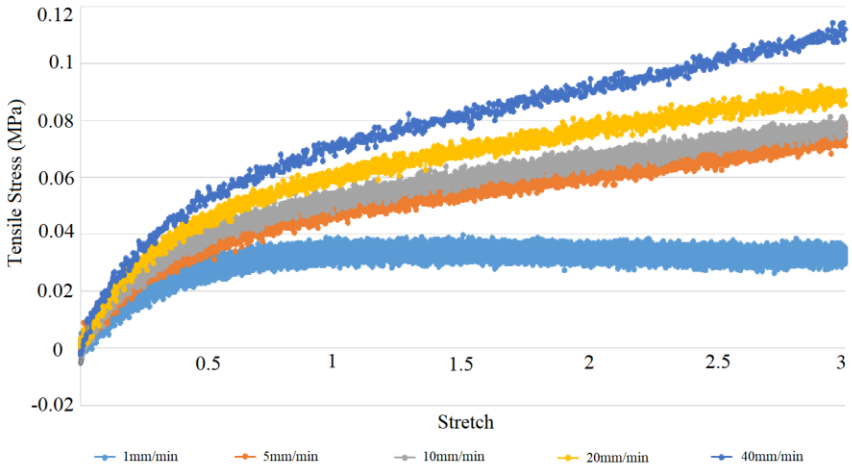

Fig.3-16. Uniaxial tensile test for 3M^{TM} VHB 4905 tape

b) Relaxation

Since the viscosity is the disturbance of the experiment, so we need to eliminate such factor. There are two ways to do so, one is to inflate the blister at a very low rate, or regardless of the inflation rate, as long as we let the inflated blister rest for enough time, the dashpot part will be fully relaxed, and the viscosity can be negligible.

We need to examine the viscoelasticity of the material by trying different stretching rate and also examine the relaxation curve after being stretched. Fig.3-17 a) shows the relaxation curve obtained both from experiment (continuous line) and mathematical simulation (discrete dots). Fig.3-17 b) shows the accurate stretch-strain curve when the sample is stretched to 400%. Same, the continuous curve is experimental, and the square dots are from the simulation.

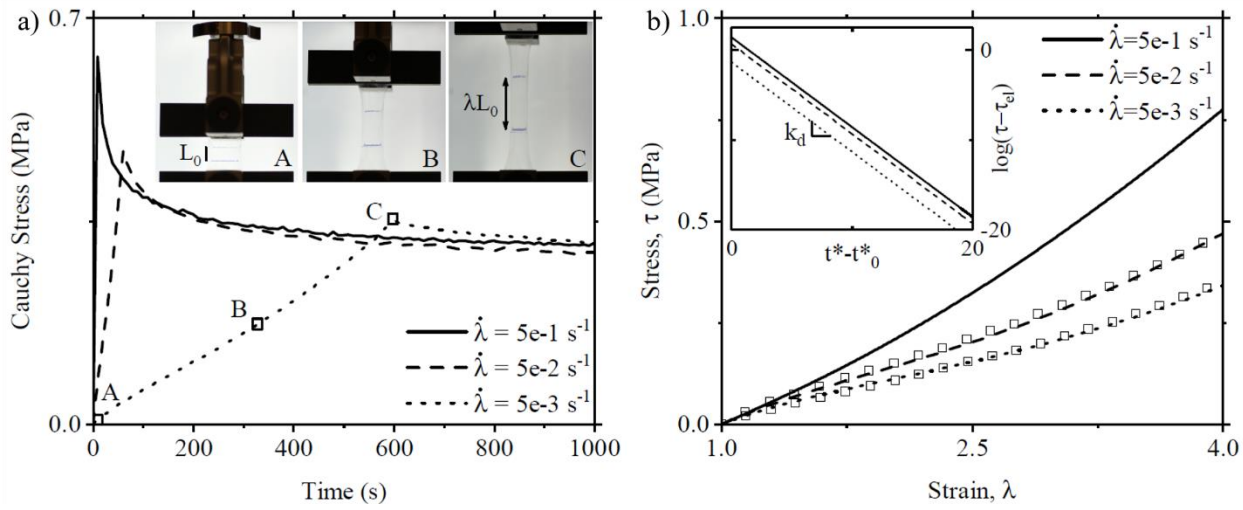

Fig.3-17. a) Relaxation curve; b) Stretch-strain cure

Regarding the blister experiments, we need to examine the repeatability of the experiment with the experiment setup. Fig.3-18 shows the pressure-volume result of 3 different experiments (inflation rate = 0.1mL/min) under same conditions, namely test 1, 2 and 3. The difference of the start point is because the preparation procedure may induce the initial pressure to the system and it is unlikely to eliminate. It is more like a tradeoff between sealing quality (sealing is necessary to prevent leaking) and the accuracy of the data. From the figure, we can see the 3 tests converges quite well despite the initial trivial differences.

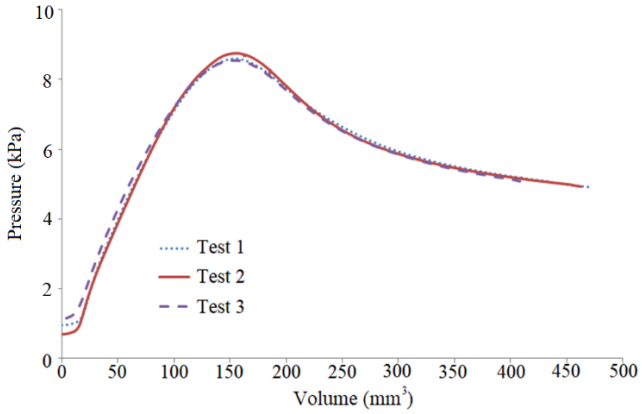

Fig.3-18. Convergence test for the whole experiment

As discussed before, the VHB tape is viscoelastic and this character will bring a whole new story of the problem. To see the viscoelasticity, we tried to load the blister at different inflation rate. The rate we choose are 0.001mL/min, 0.01mL/min, 0.05mL/min, 0.1mL/min, 1mL/min, 5mL/min, 10mL/min, 15mL/min and 20mL/min. The maximum and minimum are chosen based on the range of our equipment. An additional data is the fully relaxed data. To obtain that, we inflated the blister to different volume and let it relax for enough amount of time, then we take the end pressure as the 'relaxed data'. The results are shown in Fig.3-19. From the figure, we found that the pressure-volume data of 0.001mL/min is very close to the fully relaxed value, and the all the data converges at fully relaxed data when the inflation rate is very low and also converges when the inflation rate is very high. Another observation is that no matter what the inflation rate is, the pressure-volume curves follow the same trend at the very beginning.

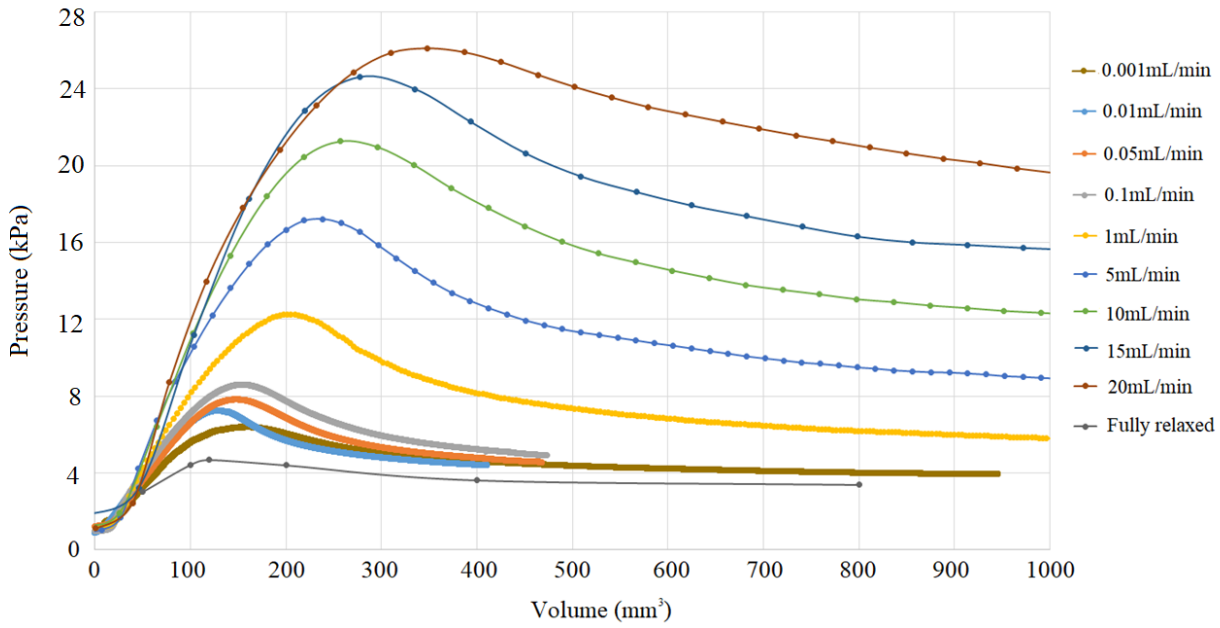

Fig.3-19. Viscoelastic test of VHB tape

c) Experimental pressure-volume data

To show the validity of the theory explained in Chapter 2.5, we first examined the pressure-volume data. In Fig.3-20 b), the solid line is the P-V data with a large W value and dot line is the one with small W value. The inflation rate we use is 1mL/min. At such rate, the viscoelasticity has an effect but since all three are under same inflation rate, the viscoelastic effect will cancel out. The general trend corresponds to the analytical results (Fig.2-11) quite well. The way we change W is by changing the temperature and setting time. According to Fig.3-20 a) [45], it only needs 1 hour to reach maximum adhesion when the temperature is 150° F (66° C) and the adhesion becomes lower as the temperature and setting time to reduce. To get the large W (also can be considered as high adhesion), we need to put the attached VHB tape in the oven at 150° F (66° C) for over an hour, and for low W (also can be considered as low adhesion) we can directly use the attached VHB tape in the room temperature with no set time. If a larger adhesion range is needed, we can change the material of the substrate according to Fig.3-20 c) [44].

d) Speculated phenomenon

From Fig.3-19, we can learn that because of the existence of viscoelasticity, the maximum pressure increases when the inflation rate increases. Therefore, we can speculate a phenomenon as following according to the graph.

In Fig.3-21, we show one scenario that could happen. The solid line represents the pressure-volume curve of no delamination circumstance. When we allow the membrane to delaminate, the dashed line will come into the picture and the place where the dashed line and solid line separates determines G_0. The bottom dash dot line represents the fully relaxed situation. Therefore, if we can inflate the blister at a very low rate, infinitely close to the fully relaxed curve, the blister will never delaminate, which means it will stay in the stable region forever. On

the contrary, when we inflate it at a high rate, i.e. the dash line, the neck radius will increase above the G_0 line and once the pressure drops below the G_0, it will be trapped there.

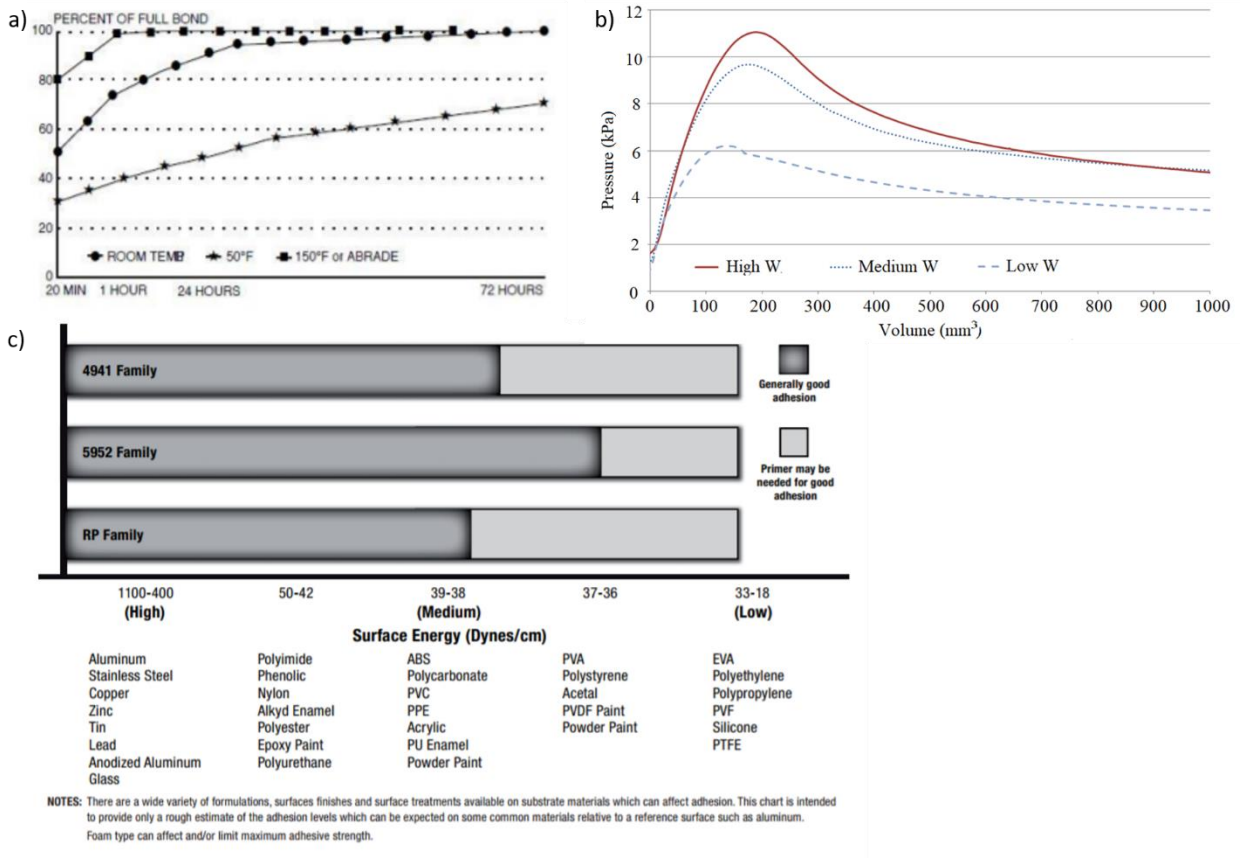

Fig.3-20. a) Adhesion graph of 3MTM VHB tape. b) Pressure-Volume data with different W value. c) Relationship of Adhesion and Surface Energy for 3M™ VHB™ Tape Adhesive Families

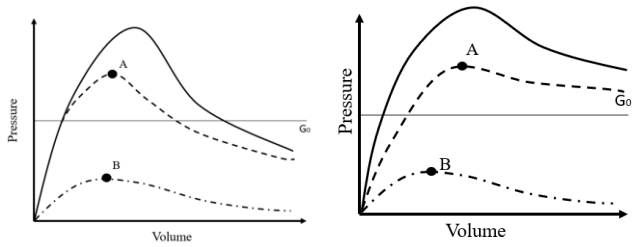

Fig.3-21. Scheme of a speculated phenomenon

Experimental validation of this theory is as follows. Firstly, we checked the critical point A and B by inflating the blister to the points via different inflation rate and stop inflating at both points and examine the delamination speed. For point A we choose the inflation speed of 2mL/min and for point B we choose 0.01mL/min. The sample is being used as soon as it is made, without any set time or heat treatment. In this experiment, a small metal cube is put right next to the blister to serve as a staff, the side length of the cube is 3mm. Fig.3-22 a) shows the delamination at point A and Fig.3-22 b) shows the delamination at point B. From the pictures, we can easily see that the point a delaminates at a very high speed while the pint B barely delaminates. This result proves the blister will delaminate fast at a high inflation rate when the pressure is above G_0 and when the pressure keeps being below G_0 the blister will be trapped.

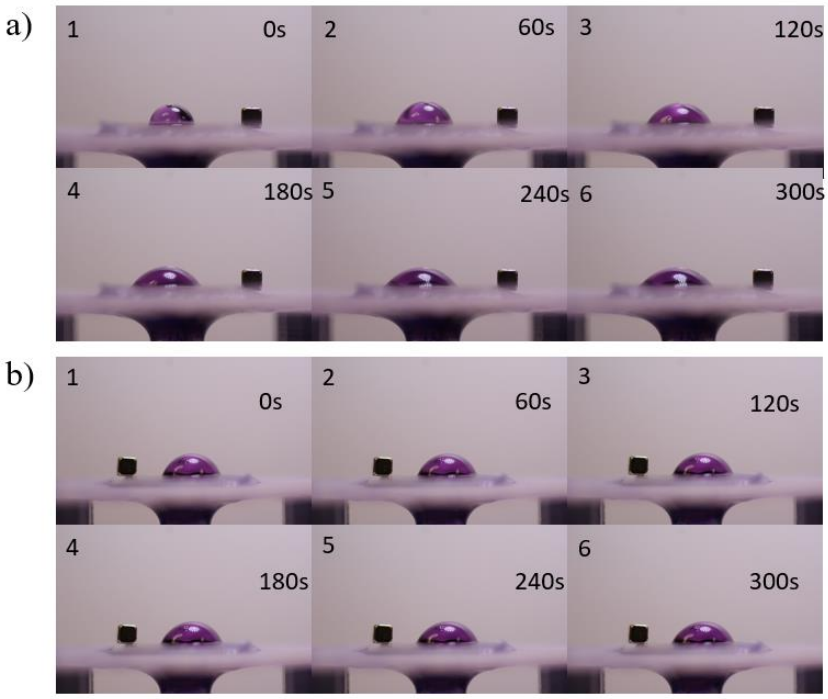

Fig.3-22. Photos of delamination at a) point A and b) point B

The other feature is to look through the scope of the whole inflating process. As predicted, the delamination should not occur throughout the process when the inflation rate is low, while the blister will either delaminate slightly at the beginning then stops to delaminate (Fig.3-21, left) or keeps delaminating (Fig.3-21, right) when the inflation rate is high. Our experiment successfully captured such behavior in Fig.3-23. In this experiment, we tried to use the slow inflation rate as 0.01mL/min and according to the pictures, the neck radius barely increases throughout the 2 hours' inflation, which means the blister is trapped.

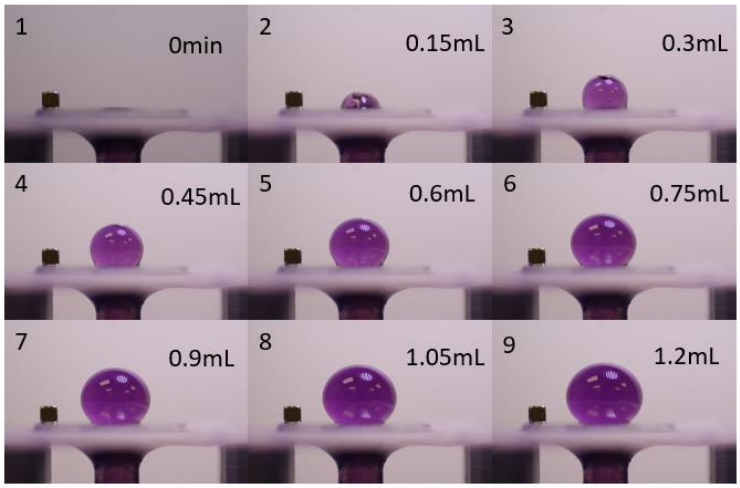

Fig.3-23. Photos for the slow inflation process

For the A points in Fig.3-21, we found that the left occasion is quite hard to get while most of the cases follow the right occasion. Despite the hardness, we still managed to produce those two scenarios. Fig.3-24 a) shows the blister is trapped again at a higher volume and Fig.3-24 b) shows the case when the blister keeps delaminating.

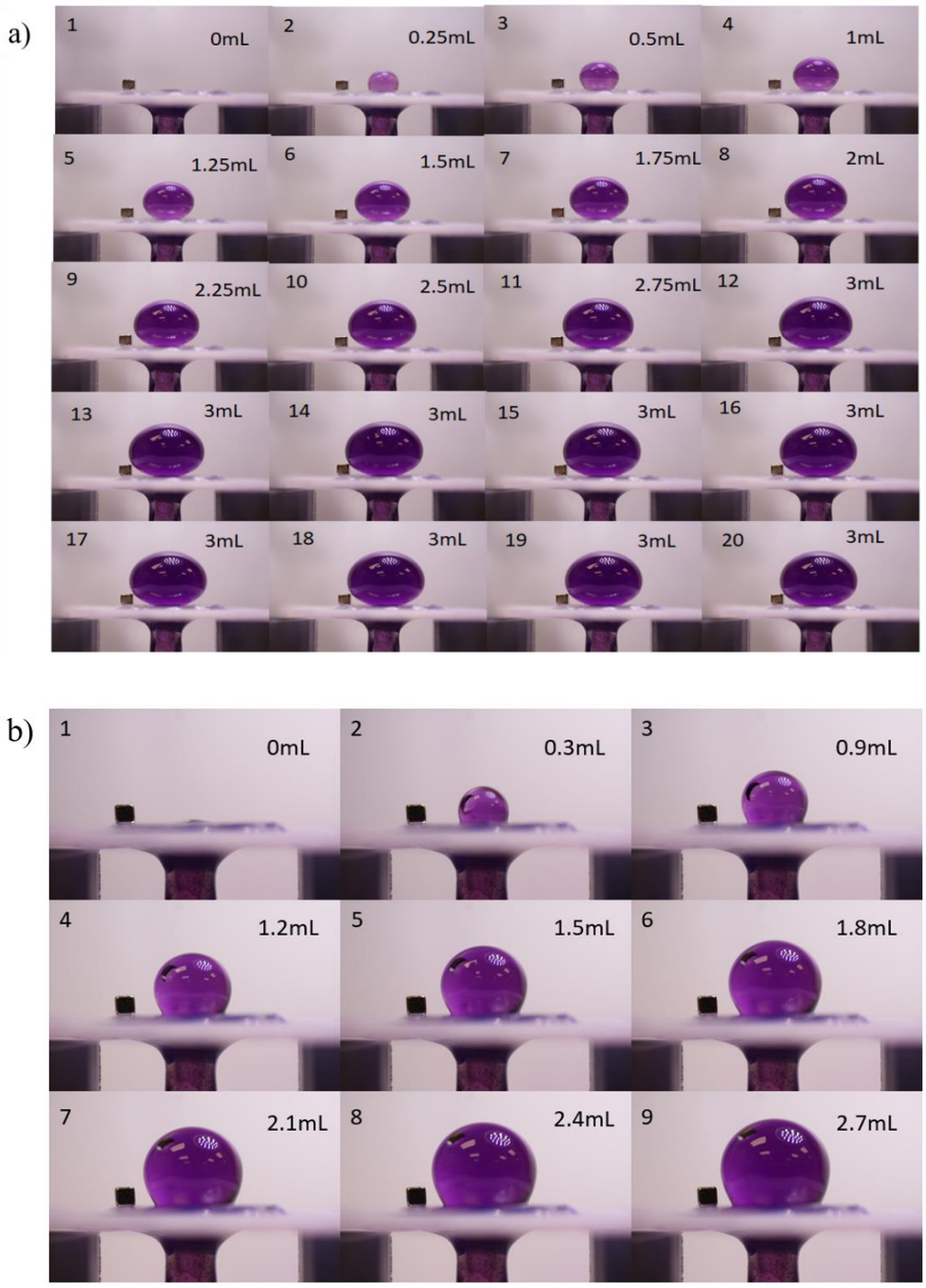

Fig.3-24. Two cases corresponding to Fig.3-18.

In Fig.3-24 b), the inflation rate was 0.5mL/min, after 12th picture, we stopped the pump and discover that the blister has been trapped. For the picture after 12, the time difference between adjacent pictures is 5 minutes.

Chapter 4

Summary and future work

In this work, we built a valid analytical model that can predict the blister growing on rigid substrate. To validate the model, we designed our own experimental system and the predictions made by the model are mostly satisfied by the experiments. From that perspective, the goal of this thesis is met. However, there are still a lot of works remain to be done. Firstly, a better material should be found to test the theory in Section 2.6, especially the phase transition process, which is the $R^* - V^*$ data. Having a better material, we can see if the blister will go through all four regions, from stable to unstable to stable region again and end up in unstable region. We will also test the influence of the inflation rate. Other than that, we need to expand the hyperelastic model to viscoelastic model and put the viscoelastic feature into the picture. Currently, we have already had some preliminary results of viscoelastic materials, while further investigation is still needed to fully complete the model.

Bibliography

1. Allen, Justine J., et al. "Cuttlefish use visual cues to control three-dimensional skin papillae for camouflage." Journal of Comparative Physiology A 195.6 (2009): 547-555.

2. G. T. Charras, M. Coughlin, T. J. Mitchison, and L. Mahadevan, Biophysical journal 94, 1836 (2008).

3. J. Nardi, T. Feder, R. Bruinsma, and E. Sackmann, Europhysics Letters (EPL) 37, 371 (1997).

4. K. T. Wan and Y. W. Mai, Acta Metallurgica Et Materialia 43, 4109 (1995).

5. J. G. Williams, International Journal of Fracture 87, 265 (1997), arXiv:arXiv:1011.1669v3.

6. N. G. Boddeti, S. P. Koenig, R. Long, J. Xiao, J. S. Bunch, and M. L. Dunn, Journal of Applied Mechanics 80, 040909 (2013), arXiv:1304.1011.

7. C. Keplinger, T. Li, R. Baumgartner, Z. Suo, and S. Bauer, Soft Matter 8, 285 (2012).

8. Fischer, W. "Über Blasenbildung bei Syringomyelie." Archiv für Dermatologie und Syphilis 113.1 (1912): 301-314.

9. Fischer, Bruno. "Über Blasenbildung bei organischen Nervenkrankheiten." Archiv für Dermatologie und Syphilis146.1 (1923): 8-13.

10. Azema, Maurice. "Le mécanisme de 1'excrétion chez les Ascidies." Compt. Rend. Acad. Sci 183 (1926): 1299.

11. Hahn, Helmut. "Ueber Hautblasenbildung." DMW-Deutsche Medizinische Wochenschrift 56.09 (1930): 353-356.

12. STOUGHTON, RICHARD B. "Mechanisms of blister formation." AMA archives of dermatology 76.5 (1957): 584-590

13. Yarnell, C. F. "Mechanism of the Formation of Blisters on the Lead Electrode of the Lead-Acid Battery." Journal of The Electrochemical Society 119.1 (1972): 19-24.

14. Nagata, Hitoshi, et al. "Blister Formation at Photoresist-Substrate Interface." Japanese journal of applied physics33.6R (1994): 3635.

15. Hinkley, J. A. "A blister test for adhesion of polymer films to SiO2." The Journal of Adhesion 16.2 (1983): 115-125.

16. Farris, T. N., and L. M. Keer. "Williams' blister test analyzed as an interface crack problem." International journal of fracture27.2 (1985): 91-103.

17. Kinloch, A. J. "Adhesives in engineering." Proceedings of the Institution of Mechanical Engineers, Part G: Journal of Aerospace Engineering 211.5 (1997): 307-335.

18. Gent, A. N., and G. R. Hamed. "Peel mechanics for an elastic-plastic adherend." Rubber Chemistry and Technology 52.5 (1979): 1057-1071.

19. Chang, Yeou-Shin, Yeh-Hung Lai, and David A. Dillard. "The constrained blister—a nearly constant strain energy release rate test for adhesives." The Journal of Adhesion 27.4 (1989): 197-211.

20. Kendall, K. "The adhesion and surface energy of elastic solids." Journal of Physics D: Applied Physics 4.8 (1971): 1186.

21. Wan, Kai-Tak, and Yiu-Wing Mai. "Fracture mechanics of a new blister test with stable crack growth." Acta metallurgica et materialia 43.11 (1995): 4109-4115.

22. Biswas, Abhijit, M. Manivannan, and Mandayam A. Srinivasan. "Multiscale layered biomechanical model of the pacinian corpuscle." IEEE transactions on haptics 8.1 (2015): 31-42.

23. Madelung, E., and S. FLUGGE. "Uber Viskoelastizitat." Annalen der Physik 22 (1935): 209-222.

24. Roy, Samit, et al. "A three-dimensional viscoelastic analysis of thin film delamination in a peninsula blister specimen." Mechanics of Advanced Materials and Structures 14.5 (2007): 379-390.

25. Camargo, C. J., et al. "Batch fabrication of optical actuators using nanotube–elastomer composites towards refreshable Braille displays." Journal of micromechanics and microengineering 22.7 (2012): 075009.

26. Lin, Sen, et al. "Shell buckling: from morphogenesis of soft matters to prospective applications." Bioinspiration & Biomimetics (2018).

27. Doi, Masao. Soft matter physics. Oxford University Press, 2013.

28. Ogden, Raymond William. "Large deformation isotropic elasticity–on the correlation of theory and experiment for incompressible rubberlike solids." Proc. R. Soc. Lond. A326.1567 (1972): 565-584.

29. Ogden, R. W. "Elastic deformations of rubberlike solids." Mechanics of solids: the Rodney Hill 60th anniversary volume. 1982. 499-537.

30. Ogden, Raymond W. Non-linear elastic deformations. Courier Corporation, 1997.

31. Yeoh, O. H. "Characterization of elastic properties of carbon-black-filled rubber vulcanizates." Rubber chemistry and technology 63.5 (1990): 792-805.

32. Bergström, J. S., and M. C. Boyce. "Deformation of elastomeric networks: relation between molecular level deformation and classical statistical mechanics models of rubber elasticity." Macromolecules 34.3 (2001): 614-626.

33. Hiermaier, S. "Sructures Under Crash and Impact." (2008).

34. https://en.wikipedia.org/wiki/Burgers_material

35. https://en.wikipedia.org/wiki/Generalized_Maxwell_model

36. Rouse Jr, Prince E. "A theory of the linear viscoelastic properties of dilute solutions of coiling polymers." The Journal of Chemical Physics 21.7 (1953): 1272-1280.

37. Likhtman, Alexei E. "Viscoelasticity and molecular rheology." Polymer Science: A Comprehensive Reference 1 (2012): 133-179.

38. Watanabe, H. "Viscoelasticity and dynamics of entangled polymers." Progress in Polymer Science 24.9 (1999): 1253-1403.

39. https://en.wikipedia.org/wiki/Strain_energy_release_rate

40. Barquins, M., and M. Ciccotti. "On the kinetics of peeling of an adhesive tape under a constant imposed load." International journal of adhesion and adhesives 17.1 (1997): 65-68.

41. Barthel, Etienne, and Stéphane Roux. "Velocity-dependent adherence: an analytical approach for the JKR and DMT models." Langmuir 16.21 (2000): 8134-8138.

42. Mangan, Robert, and Michel Destrade. "Gent models for the inflation of spherical balloons." International Journal of non-linear mechanics 68 (2015): 52-58.

43. http://multimedia.3m.com/mws/media/764998O/iatd-product-info.pdf

44. https://multimedia.3m.com/mws/media/67100O/3mtm-vhb-tapes.pdf

45. https://multimedia.3m.com/mws/media/66019O/vhbtm-tape-surface-preparation-technical-bulletin.pdf

46. Simo, Juan C., and David D. Fox. "On a stress resultant geometrically exact shell model. Part I: Formulation and optimal parametrization." Computer Methods in Applied Mechanics and Engineering 72.3 (1989): 267-304.

47. Chen, Hang, et al. "Experiments and viscoelastic analysis of peel test with patterned strips for applications to transfer printing." Journal of the Mechanics and Physics of Solids 61.8 (2013): 1737-1752.

48. Long, Rong, Kenneth R. Shull, and Chung-Yuen Hui. "Large deformation adhesive contact mechanics of circular membranes with a flat rigid substrate." Journal of the Mechanics and Physics of Solids 58.9 (2010): 1225-1242.